UNIVERSITY OF HELSINKI REPORT SERIES IN PHYSICS

HU-P-D158

Heavy-light mesons on a lattice

JONNA KOPONEN

Division of Elementary Particle Physics
Department of Physics
Faculty of Science
University of Helsinki
Helsinki, Finland

ACADEMIC DISSERTATION
To be presented, with the permission of the Faculty of Science of the University of Helsinki, for public criticism in the Small Auditorium (E204) of Physicum, Gustaf Hällströmin katu 2, on Friday, May 8th, 2009, at 10 o'clock.

Helsinki 2009

Cover picture:
Mika Jahma

ISBN 978-952-10-4227-0 (printed version)
ISSN 0356-0961
ISBN 978-952-10-4228-7 (pdf-version)
http://ethesis.helsinki.fi
Yliopistopaino
Helsinki 2009

Preface

This thesis is based on research carried out at the Department of Physics in the University of Helsinki. I have also been an adjoint member of Helsinki Institute of Physics (HIP). The work was financially supported by the Magnus Ehrnrooth Foundation, the Finnish Cultural Foundation and the Academy of Finland (contract numbers 177881 and 54038), which is gratefully acknowledged. This work was supported in part by the EU grant HPRN-CT-2002-00311, "Euridice" and the EU Contract No. MRTN-CT-2006-035482, "FLAVIAnet". I also wish to thank the UKQCD Collaboration for providing the lattice configurations, and the CSC – IT Center for Science Ltd in Espoo, Finland, for making available the computer resources.

I am very grateful to my supervisor Anthony Green for guidance and support. Thank you! I wish to thank Chris Michael and Petrus Pennanen for good collaboration — it has been a pleasure to work with you. My thanks go out also to Janne Ignatius and Mika Jahma, who coded the program for the Dirac model. I would also like to express my gratitude to the referees of my thesis, Prof. Kari Rummukainen and Dr. Arttu Rajantie, for their constructive and very helpful comments. I have enjoyed my time at the Department of Physics, and I want to say thank you to all coworkers collectively. Special thanks go to Keijo Kajantie and Mikko Sainio, who have helped me in numerous ways during my studies. Last, but not least, I wish to thank my family for support and encouragement.

Helsinki, March 2009

Jonna Koponen

J. Koponen: Heavy-light mesons on a lattice, University of Helsinki, 2009, 70 p. + appendices, University of Helsinki, Report Series in Physics, HU-P-D158, ISSN 0356-0961, ISBN 978-952-10-4227-0 (printed version), ISBN 978-952-10-4228-7 (pdf version).
INSPEC classification: A1110C, A1110N, A1235E, A1240Q, A1440M.
Keywords: quantum chromodynamics, B mesons, lattice QCD.

Abstract

Several excited states of D_s and B_s mesons have been discovered in the last six years: BaBar, Cleo and Belle discovered the very narrow states $D^*_{s0}(2317)^\pm$ and $D_{s1}(2460)^\pm$ in 2003, and CDF and DØ Collaborations reported the observation of two narrow B_s resonances, $B_{s1}(5830)^0$ and $B^*_{s2}(5840)^0$ in 2007. To keep up with experiment, meson excited states should be studied from the theoretical aspect as well.

The theory that describes the interaction between quarks and gluons is quantum chromodynamics (QCD). In this thesis the properties of the meson states are studied using the discretized version of the theory — lattice QCD. This allows us to perform QCD calculations from first principles, and "measure" not just energies but also the radial distributions of the states on the lattice. This gives valuable theoretical information on the excited states, as we can extract the energy spectrum of a static-light meson up to D wave states (states with orbital angular momentum $L = 2$). We are thus able to predict where some of the excited meson states should lie. We also pay special attention to the order of the states, to detect possible inverted spin multiplets in the meson spectrum, as predicted by H. Schnitzer in 1978. This inversion is connected to the confining potential of the strong interaction.

The lattice simulations can also help us understand the strong interaction better, as the lattice data can be treated as "experimental" data and used in testing potential models. In this thesis an attempt is made to explain the energies and radial distributions in terms of a potential model based on a one-body Dirac equation. The aim is to get more information about the nature of the confining potential, as well as to test how well the one-gluon exchange potential explains the short range part of the interaction.

Contents

List of included papers

The four articles included in this thesis are [1, 2, 3, 4]:

[1] A. M. Green, J. Koponen, C. Michael, P. Pennanen, *The Charge and matter radial distributions of heavy light mesons calculated on a lattice*,
PRD **65** (2002) 014512,[hep-lat/0105027].
URL: http://link.aps.org/doi/10.1103/PhysRevD.65.014512

[2] A. M. Green, J. Koponen, C. Michael, P. Pennanen, *The Charge and matter radial distributions of heavy light mesons calculated on a lattice with dynamical fermions*,
EPJC **28** (2003) 79, [hep-lat/0206015].

[3] A. M. Green, J. Koponen, C. McNeile, C. Michael, G. Thompson, *Excited B mesons from the lattice*,
PRD **69** (2004) 094505, [hep-lat/0312007].
URL: http://link.aps.org/doi/10.1103/PhysRevD.69.094505

[4] J. Koponen, *Energies of B_s meson excited states: A lattice study*,
PRD **78** (2008) 074509, [0708.2807 (hep-lat)].
URL: http://link.aps.org/doi/10.1103/PhysRevD.78.074509

Author's contribution

Paper [1]:
In the first paper we studied the heavy-light mesons on a quenched lattice. Michael and Peisa had developed a new method — maximal variance reduction — for calculating better estimates for quark propagators. They used small lattices, $8^3 \times 24$ and $12^3 \times 24$, to demonstrate the method and extract the energies of heavy-light meson excited states. We thus continued their work and, collaborating with Chris Michael, measured the energies on a larger $16^3 \times 24$ lattice. A static heavy quark also allows one to explore the light quark distribution around it. We thus extended the study by adding a probe and measuring the vector (charge) and scalar (matter) distributions and the corresponding sum rules for the S wave state. A large part of the paper is devoted to the analysis of the radial distributions. My contribution to this paper was doing the lattice measurements (i.e. computer simulations), as well as analysing the data and writing the paper jointly with all collaborators.

Paper [2]:
The second paper continued the study of heavy-light meson radial distributions. The new development was using dynamical fermions, and comparing these unquenched results to earlier quenched results. Many off-axis data points were also added to the radial distribution measurements. The emphasis was on the analysis of the S wave charge and matter distributions. The analysis of the data and writing of the paper was done jointly with all collaborators. I was responsible for doing the measurement runs on CSC computers.

Paper [3]:
In the third paper we concentrated on extracting the energy spectrum up to F wave states using new unquenched lattices, and comparing the results to the quenched results from the first paper. We used lattices with different hopping parameters (i.e. different light quark masses), so that we were able to study how the meson mass depends on the light quark mass. We paid special attention in determining where the P wave states lie, and predicted that they lie near the BK and B^*K thresholds and can hence be expected to be narrow. As in the previous papers, my contribution was doing the lattice measurements as well as analysing the data and writing the paper jointly with all collaborators.

Paper [4]:
The fourth paper concentrated on improving the lattice measurements of the energy spec-

trum of the heavy-light meson. In this paper smearing was introduced in the time direction to get a better signal to noise ratio. Otherwise the lattice configurations were the same as in the previous paper, except that one new lattice with a smaller light quark mass was also used in the study. Special attention was paid in extracting the spin-orbit splittings. The simulations, analysis of the data and the actual writing of the paper was done by me, with kind help (discussions, reading the manuscript) from my supervisor Anthony Green and collaborator Chris Michael.

Chapter 1

Introduction

The topic of interest here is heavy-light mesons, i.e. particles that consist of a heavy quark and a light anti-quark (or vice versa). We wish to study some properties of these mesons starting from the underlying theory, quantum chromodynamics (QCD), that describes the interactions of quarks and gluons. Although we approach the topic from a theoretical viewpoint, such heavy-light mesons can be (and have been) observed in experiments: for example in a B meson, the b quark is about 1000 times as heavy as the accompanying u or d quark, and the meson can thus be considered as a heavy-light system. The suggested $q\bar{q}$ quark-model assignments for some of the light-light and heavy-light mesons are given in Table 1.1.

The heavy-light meson is one of the most fundamental systems in QCD (like the hydrogen atom in QED), but has interparticle correlations that are little understood. We wish to use the properties of these meson states to gain some knowledge of the interaction between the quarks. The excited B meson states also have important applications to CP studies of neutral B mesons by the identification of their flavour (b versus $\bar{b}$) through the decay chain $B^* \to B^0\pi^\pm$ ([6]). Hence narrow B^* resonances will be valuable for this. However, not many of these excited states have so far been observed in experiments.

In 2003 BaBar, Cleo and Belle discovered that the $c\bar{s}$ states with $J^P = 0^+$ and 1^+ (where J is total angular momentum and P is parity) have very narrow widths [7, 8, 9]. This naturally raised the question of whether the corresponding $b\bar{s}$ states will also be narrow. The main reason for the narrow width of these D_s meson states is that the transition to DK is not energetically allowed (for the $D^*_{s0}(2317)^\pm$ state) or the state is close to a threshold (for the $D_{s1}(2460)^\pm$ state). Thus the only allowed hadronic decay proceeds via isospin-violation (since $m_u \neq m_d$) to $D_s\pi$ and so the state will have a very small width. Likewise, if the equivalent $b\bar{s}$ states are close to or below the BK threshold, then they

Meson	Quark structure	I	Energy [MeV]
π	$u\bar{d}$, $(u\bar{u}-d\bar{d})/\sqrt{2}$, $d\bar{u}$	1	135
ρ	$u\bar{d}$, $(u\bar{u}-d\bar{d})/\sqrt{2}$, $d\bar{u}$	1	775
ω	$c_1(u\bar{u}+d\bar{d})+c_2(s\bar{s})$	0	783
ϕ	$c_3(u\bar{u}+d\bar{d})+c_4(s\bar{s})$	0	1019
K	$u\bar{s}$, $d\bar{s}$, $s\bar{u}$, $s\bar{d}$	1/2	494
D	$c\bar{d}$, $c\bar{u}$, $d\bar{c}$, $u\bar{c}$	1/2	1865
D_s	$c\bar{s}$, $s\bar{c}$	0	1968
B	$b\bar{d}$, $b\bar{u}$, $d\bar{b}$, $u\bar{b}$	1/2	5279
B_s	$b\bar{s}$, $s\bar{b}$	0	5366

Table 1.1: The suggested $q\bar{q}$ quark-model assignments for some of the light-light and heavy-light mesons. I is the isospin of the meson, and "Energy" is the experimental energy of the lowest lying state (to the nearest MeV) [5].

will be very narrow. In 2007 CDF and DØ Collaborations reported the observation of two narrow B_s resonances, that are associated with the $J^P = 2^+$ and 1^+ states [10, 11, 12]. However, the other two P wave states with $J^P = 0^+$ and 1^+ have not been observed yet. Therefore, the main focus of this work is to use a theoretical approach and predict where these $b\bar{s}$ states should lie and, in addition, extract the form of their radial structure. The latter have not been studied before with the present approach.

Several properties of a given meson state, such as its energy, width and angular momentum, can often be determined experimentally. However, usually the experiments give no information of the structure of the state. For example, with B_s states the experiments do not tell whether the measured states are $b\bar{s}$, $b\bar{s}u\bar{u}$ or BK. Unfortunately, when theoretical models are constructed attempting to describe B_s states, it usually has to be decided beforehand which structure is used for the states. The models have often sufficient freedom to fit experimental data with any of the possible structures. Therefore, if — for example — transition rates between states in a heavy-light meson ($Q\bar{q}$) are calculated, then the necessary radial wave functions are simply taken to have some convenient form, or are calculated with a differential equation and interquark interaction that are not well justified.

In an attempt to clarify the comparison between the experimental data and theory, we suggest the use of lattice QCD. In practice, there are two ways to perform QCD calculations: use perturbation theory, or discretize the theory and do the calculations numerically on a computer (lattice QCD). Perturbation theory is valid at high energies, and QCD has

been well tested in high energy scattering experiments. However, at low energies perturbation theory is not applicable. Lattice QCD allows us to do QCD calculations from first principles, and we can get information of the energy spectrum of the mesons as well as the structure of the states. It gives us the possibility to do "measurements" and get lots of data that can be treated as experimental data. This lattice data can then be used to test theoretical models. We have chosen to study static-light mesons, i.e. mesons where the heavy quark is static (infinitely heavy), as it provides a good test environment for model building. The ultimate goal would be to be able to understand and describe multi-quark systems: In [13, 14, 15, 16] A. M. Green, C. Michael and collaborators studied two and four static quark systems on a lattice, and in [17] a system of two static-light mesons was studied. The emphasis was in gaining knowledge of the multi-quark interactions. However, it is beneficial to study the more simple $Q\bar{q}$ system first, and hopefully use this information in future multi-quark studies.

This thesis is organized as follows: In Chapter 2 the basic concepts of lattice QCD are introduced briefly. Our results are presented in Chapters 3 (energy spectrum and spin-orbit splitting) and 4 (radial distributions and sum rules). In Chapter 5 we construct a model based on a one-body Dirac equation that can be used to try to describe the data. The conclusions in Chapter 6 close the thesis.

Chapter 2

Brief introduction to lattice QCD

Let us start by introducing the main ideas of lattice QCD very briefly. The basic Lagrangian of QCD is

$$\mathcal{L}_{\text{QCD}} = \mathcal{L}_{\text{fermions}} + \mathcal{L}_{\text{gauge}}, \tag{2.1}$$

where the gauge part (using Euclidean metric $g^{\mu\nu} = \delta^{\mu\nu}$)

$$\mathcal{L}_{\text{gauge}} = \frac{1}{4} F^a_{\mu\nu} F^{\mu\nu}_a, \qquad F^a_{\mu\nu} = \partial_\mu A^a_\nu - \partial_\nu A^a_\mu + g f^{abc} A^b_\mu A^c_\nu, \tag{2.2}$$

describes the propagation of gluons and their self-interactions, and the fermionic part

$$\mathcal{L}_{\text{fermions}} = \sum_f \bar{\psi}^f (\not{D} + m^f) \psi^f \tag{2.3}$$

with the covariant derivative

$$\not{D} = i\gamma_\mu (\partial_\mu - i g A^a_\mu T^a) \tag{2.4}$$

describes the propagation of quarks and their interaction with the gauge field $A_\mu = A^a_\mu T^a$. Here a, b and c are colour indices that run from 1 to $N_c^2 - 1$, if the colour group is $\text{SU}(N_c)$. In the physical case the group is SU(3), as there are three colours. The T^a are the generators of the group that satisfy

$$[T^a, T^b] = i f^{abc} T^c \tag{2.5}$$

and are normalized as

$$\text{Tr}(T^a T^b) = \frac{1}{2} \delta^{ab}, \tag{2.6}$$

where f^{abc} are the structure coeffcients. The μ and ν are Lorentz indices that identify the spatial and temporal components of the vector gauge fields. f is the flavour index for the quarks. Here the Dirac and colour indices of the spinors ψ^f have been suppressed.

As the Lagrangian is known, we can in principle write down an expression for any quantity we wish to compute. If, for example, we want to compute some property of a bound state, we have to evaluate a path integral

$$\langle B \rangle = \frac{1}{\mathcal{Z}} \int \mathcal{D}A_\mu \int \mathcal{D}\psi \int \mathcal{D}\bar{\psi} B \, \mathrm{e}^{-S}, \tag{2.7}$$

where

$$\mathcal{Z} = \int \mathcal{D}A_\mu \int \mathcal{D}\psi \int \mathcal{D}\bar{\psi} \, \mathrm{e}^{-S} \tag{2.8}$$

and the action is

$$S = \int \mathrm{d}^4 x \, \mathcal{L}_{\mathrm{QCD}}. \tag{2.9}$$

The path integral is defined in Euclidean space, where the time $t \to -it$, to get a convergent measure. The operator B is given in terms of the fermion and gauge fields, and it is defined by the property of the state we are interested in. A typical example would be the energy of a bound state.

Even though the task has been reduced to evaluating the integral in Eq. (2.7), this is easier said than done. In the study of high energy phenomena, the coupling g is sufficiently small to justify an expansion in powers of g. However, in the study of the properties of hadrons, e.g. their energies and radial distributions, as in the present study, the coupling $g \approx 1$. This rules out perturbative approach and necessitates the use of purely numerical methods. Therefore, to calculate the integral in Eq. (2.7) the time and space are discretized, so that we get a four dimensional grid. This discretization actually simply gives a precise meaning to the path integrals. In field theory one has an infinite number of degrees of freedom, so the integrals have to be regularized (by introducing the lattice). This is the first step in the renormalization program [18]. The second step is removing the lattice structure, i.e. studying the continuum limit to return to the real world. The grid, or lattice, is typically of size $16^3 \times 24$ or even $24^3 \times 48$ in QCD calculations. The gauge fields U_μ are on the links and the fermion fields ψ on the sites of the lattice. The connection between the two gauge fields, U_μ on the lattice and A_μ in the continuum theory, is made via a path ordered integral

$$U_\mu(x) = P \exp\left[g i \int_x^{x + a\hat{e}_\mu} \mathrm{d}y_\nu A_\nu(y) \right]. \tag{2.10}$$

The lattice action can be written as

$$S[U, \bar{\psi}, \psi] = S_G[U] + S_F[U, \bar{\psi}, \psi], \tag{2.11}$$

where

$$S_G[U] = \beta \sum_P \left(1 - \frac{1}{N_c} \operatorname{Re} \operatorname{Tr} U_P \right) \tag{2.12}$$

is the Wilson plaquette action for the gauge fields, and the fermionic part S_F is defined by

$$S_F[U,\bar{\psi},\psi] = S_F^W[U,\bar{\psi},\psi] - c_{\rm SW}\frac{i\kappa}{2}\sum_{x,\mu,\nu}\bar{\psi}_x\sigma_{\mu,\nu}F_{\mu,\nu}(x)\psi_x. \tag{2.13}$$

Here S_F^W is the standard Wilson action for fermions and $c_{\rm SW}$ denotes the improvement coefficient multiplying the Sheikholeslami–Wohlert term [19]. The standard Wilson action for fermions is

$$S_F^W[U,\bar{\psi},\psi] = \sum_x\left[\kappa\sum_\mu\left\{\bar{\psi}_x(\gamma_\mu-1)U_\mu(x)\psi_{x+\mu} - \bar{\psi}_{x+\mu}(\gamma_\mu+1)U_\mu^\dagger(x)\psi_x\right\} + \bar{\psi}_x\psi_x\right]. \tag{2.14}$$

The action is named after K. G. Wilson, who introduced the idea of discretization (lattice) in the 1970's [20]. The purpose of the Sheikholeslami–Wohlert term is to remove the $\mathcal{O}(a)$ lattice artifacts, so that the remaining effects are of second order (a^2) or higher in the lattice spacing a. This is important, as the calculations are done on a fixed, non-zero lattice spacing, and ideally the results have to be extrapolated to the continuum limit.

The parameters of the theory are the gauge coupling $\beta \equiv 2N_c/g^2$ (g is the usual coupling) and the hopping parameter κ. The hopping parameter is a simple rescaling factor that is related to the quark mass m_q via

$$\kappa = \frac{1}{2(4+m_q)} \tag{2.15}$$

at tree level [21]. Typical values are $\beta = 6.2$, $\beta = 5.2$ and $\kappa = 0.141$, $\kappa = 0.135$, depending on whether the lattice is quenched (no quark-antiquark loops) or unquenched (dynamical fermions, i.e. quark-antiquark loops allowed). The nonperturbatively $\mathcal{O}(a)$ improved Wilson action was determined in the quenched approximation in Refs. [22, 23], and first results for $n_f = 2$ flavors of dynamical quarks were reported in [24]. Some of the lattice configurations used in this study use $c_{\rm SW} = 1.76$ for the improvement (clover) coefficient. This was a preliminary estimate provided by the ALPHA Collaboration prior to their final result $c_{\rm SW} = 2.017$ at $\beta = 5.2$, presented in [24]. Note that the lattice spacing a is not a free parameter, but depends on the coupling β. The value of a is extracted from a lattice measurement. Usually experimental input is used to set the scale: The mass of the ρ meson can be calculated on the lattice, and matching that to the experimental result can be used to set the lattice spacing. The masses of K, K^* or ϕ mesons are often used to calculate the strange quark mass [21].

It should also be noted that the discretization is not unambiguous or unique: different discretizations can be used, and it depends on the task at hand what kind of discretization is most convenient. However, in the continuum limit the discretized theory has to give

the correct continuum theory. In our work we use the above mentioned standard Wilson action for the gauge fields and clover (Sheikholeslami–Wohlert improved Wilson) action for the fermions. Also the discretization can be further improved by so-called fuzzing, where the original link is replaced by a certain combination of the neighbouring links. A very commonly used fuzzing simply sums the four "staples" that are connected to the given link, i.e. the fuzzed link $\tilde{U}_{i,\mu}$ is calculated as

$$\tilde{U}_{i,\mu} = \mathrm{Proj}_{\mathrm{SU(3)}}\left[b_1 U_{i,\mu} + b_2 \sum_{\pm\eta\neq\mu} U_{i,\eta} U_{i+\hat{\eta},\mu} U^{\dagger}_{i+\hat{\mu},\eta} \right]. \tag{2.16}$$

Here $U_{i,\mu}$ is the original, unfuzzed link at location i and spatial direction μ (also η is in spatial direction). The coefficients b_1 and b_2 can be tuned according to the task at hand. Often several iterations of fuzzing are used. See also Section 3.2 (specifically Fig. 3.2 — the APE smearing is essentially standard fuzzing in the time direction).

Lattice QCD calculations are nowadays a huge industry. It is impossible to cover all topics here, and that is not the purpose of this thesis either. Interested readers can find detailed introduction to lattice field theories in many text books, for example by Montvay and Münster [25] and Rothe [18]. Ref. [26] is a collection of five long articles on different topics of lattice QCD, and the target audience is advanced undergraduates and graduate students who have background in nuclear and/or particle physics.

Chapter 3

Energy spectrum

Our aim is to extract (i.e. measure) the energies of both angular and first radial excitations of heavy-light mesons on the lattice. We use several different lattices to get as broad a picture as possible. Quenched measurements are done on $12^3 \times 24$ and $16^3 \times 24$ lattices, and later unquenched measurements on $12^3 \times 24$, $16^3 \times 24$, $12^3 \times 32$ and $16^3 \times 32$ lattices with two degenerate quark flavours. The quenched lattices are labelled as "Q1", "Q2", "Q3", and the unquenched lattices (i.e. lattices with dynamical fermions) are labelled as "DF1", "DF2", "DF3", "DF4", "DF5". Quenched lattices have the gauge coupling $\beta = 5.7$, whereas the unquenched lattices have $\beta = 5.2$. The lattices have different lattice spacings and light quark masses. Detailed information on the lattice parameters

	β	c_{SW}	κ	r_0/a	# of confs.	Size $(L^3 \times T)$
Q1	5.7	1.57	0.14077	2.94	20	$12^3 \times 24$
Q2	5.7	1.57	0.13843	2.94	20	$12^3 \times 24$
Q3	5.7	1.57	0.14077	2.94	20	$16^3 \times 24$
DF1	5.2	1.76	0.1395	3.435^{+48+42}_{-47-0}	20	$12^3 \times 24$
DF2	5.2	1.76	0.1395	3.444^{+40+26}_{-57-78}	78	$16^3 \times 24$
DF3	5.2	2.017	0.1350	$4.754(40)^{+2}_{-90}$	160	$16^3 \times 32$
DF4	5.2	2.017	0.1355	$5.041(40)^{+0}_{-10}$	119	$16^3 \times 32$
DF5	5.2	2.017	0.1358	5.32(5)	139	$16^3 \times 32$

Table 3.1: Lattice parameters (from [27, 28, 29, 30]). The Sommer scale parameter can be taken to be $r_0 = 0.525(25)$ fm. The error on r_0/a for the quenched lattices is not given in the publications. See Chapter 2 for definitions of β, c_{SW} and κ [Eqs. (2.12), (2.13), (2.15)]. The column "# of confs." is the number of gauge configurations.

are given in Table 3.1, and lattice spacings, masses and other similar quantities are given in Table 3.2. The parameters κ and β are usually chosen so that one gets as small lattice spacing and light quark masses as possible - the restricting factor being the computer time. Our main results on the energy spectrum are published in [3, 4], whereas [1] and [2] concentrate more on the radial distributions.

The lattice spacings range from approximately 0.17 fm to 0.1 fm, and the light quark masses range from $1.1m_s$ to $0.3m_s$, where m_s is the strange quark mass. All lattice configurations were generated by the UKQCD Collaboration. More details of the lattice configurations used in this study can be found in Refs. [3, 27, 28, 29, 30]. Because our light quarks are heavier than true u and d quarks, we have m_π ranging from 810 MeV to 400 MeV.

3.1 Excited state operators and two-point correlation functions

When the heavy quark is taken to be static (infinitely heavy), the $\bar{Q}q$ meson becomes the "hydrogen atom" of QCD. Charge conjugation is not a good quantum number, because the two quarks are not identical. Since the heavy quark spin does not play a role, we may

	a [fm]	$r_0 m_\pi$	m_π [MeV]	m_π/m_ρ	m_q
Q1	0.18	1.555(6)	584	0.715	$0.9m_s$
Q2	0.18	2.164(6)	813	0.757	$1.8m_s$
Q3	0.18	1.555(6)	584	0.715	$0.9m_s$
DF1	0.15	1.92(4)	722	0.710	$1.3m_s$
DF2	0.15	1.94(3)	730	0.719	$1.3m_s$
DF3	0.11	1.93(3)	725	0.700	$1.1m_s$
DF4	0.10	1.48(3)	556	0.578	$0.6m_s$
DF5	0.10	1.06(3)	398	0.440	$0.3m_s$

Table 3.2: Lattice parameters (from [27, 28, 29, 30]). The Sommer scale parameter can be taken to be $r_0 = 0.525(25)$ fm. Often the m_π/m_ρ is quoted to give a feeling of how heavy or light the lattice quarks are. For comparison, if the m_π and m_ρ were made of s-quarks, the ratio would be about 0.7. Here m_s is the strange quark mass, which the Particle Data Group [5] quotes as 104^{+26}_{-34} MeV.

label the states with $j = \mathrm{L} \pm \frac{1}{2}$ as $\mathrm{L}_\pm$. Here L is the orbital angular momentum and $\pm\frac{1}{2}$ refers to the spin of the light quark. For example, the state with L=1 and anti-aligned angular momentum and light quark spin is $\mathrm{P}_- = \mathrm{P}_{1/2}$. The corresponding state with aligned light quark spin and angular momentum is $\mathrm{P}_+ = \mathrm{P}_{3/2}$. Going away from the heavy quark static limit breaks the degeneracy to give the four states $J^P = 0^+, 1^+$ (P_-) and $J^P = 1^+, 2^+$ (P_+) seen in nature. In addition to the states labelled $\mathrm{L}_\pm$, we also study states that are mixtures of the two spin states. These are labelled L_{+-}.

We use the same lattice operators to construct these states that were used in [27] and [31]. Nonlocal operators are used for the heavy-light meson, because that enables us to study also the orbital excitations. The lattice operator is defined on a timeslice t as

$$B_t = \sum_{\mathbf{x}_1, \mathbf{x}_2} \bar{Q}(\mathbf{x}_2, t) P_t(\mathbf{x}_1, \mathbf{x}_2) \Gamma q(\mathbf{x}_1, t). \tag{3.1}$$

Here Q and q are the heavy and light quark fields respectively, the sums are over all space at a given time t. P_t is a linear combination of products of gauge links U at time t along paths P from $\mathbf{x}_1$ to $\mathbf{x}_2$, and Γ defines the spin structure of the operator. For pseudoscalar mesons, the only ones studied here, $\Gamma = \gamma_5$. The Dirac spin indices and the colour indices are suppressed for clarity.

The 2-point correlation function $C_2(T)$ (see Fig. 3.1) is defined as $B_t \bar{B}_{t+T}$, i.e. the meson is created at time t and destroyed at time $t + T$. More explicitly, the 2-point correlator is

$$C_2(T) = \mathrm{Tr} \left\langle P_t \Gamma G_q(\mathbf{x'}_1, t+T, \mathbf{x}_1, t) P_{t+T} \Gamma^\dagger G_Q(\mathbf{x}_2, t, \mathbf{x'}_2, t+T) \right\rangle . \tag{3.2}$$

In the case of a static heavy quark, the heavy quark propagator G_Q is

$$G_Q(\mathbf{x}_2, t, \mathbf{x'}_2, t+T) = \frac{1}{2}(1+\gamma_4) U^Q(\mathbf{x}_2, t, T) \delta_{x_2, x'_2}, \tag{3.3}$$

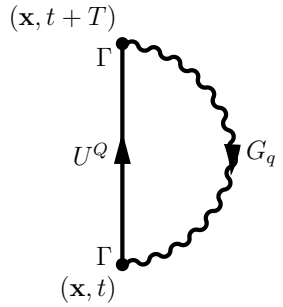

Figure 3.1: Two-point correlation function.

where

$$U^Q(\mathbf{x}, t, T) = \prod_{i=0}^{T-1} U_4(\mathbf{x}, t+i). \tag{3.4}$$

In other words, if the heavy quark is infinitely heavy, the propagator is simply a product of the gauge links $U_4(\mathbf{x}, t)$ from time t to $t+T$. The light anti-quark propagator $G_q(\mathbf{x}, t+T, t)$ is evaluated using stochastic methods (see [27] for more details) as

$$(G_q)_{ij} = Q^{-1}_{ij} = \langle (Q_{ik}\psi_k)^* \psi_j \rangle, \tag{3.5}$$

where Q is the Wilson–Dirac fermion matrix [basically $1 - \kappa M$ plus the Sheikholeslami–Wohlert term, i.e. the fermion action given in Eq. (2.13)], ψ are the fermion fields and $\langle ... \rangle$ denotes an average over the stochastic samples. Using these in Eq. (3.2) gives

$$C_2(T) = \mathrm{Tr} \left\langle P_t \Gamma \psi(\mathbf{x'}_1, t+T) [Q\psi(\mathbf{x}_1, t)]^* P_{t+T} \Gamma^\dagger \frac{1}{2}(1+\gamma_4) U^Q(\mathbf{x}_2, t, T) \right\rangle . \tag{3.6}$$

Here the trace is over Dirac and colour indices, and includes also the spatial sums.

The b quarks are usually described as heavy, as their mass is significantly greater than the QCD scale: $m_b \approx 4.5$ GeV compared to $\Lambda_{\mathrm{QCD}} \approx 300$ MeV. They are non-relativistic in the bound states, and $\alpha(m_Q)$ is relatively small. The b quarks could, in principle, be treated on the lattice the same way as the light quarks, but that would introduce a new problem. The lattice spacing has to be small enough, $a \ll 1/m_Q$, or otherwise the size of the quark is smaller than a, i.e. the quark would "fall through the lattice grid". Treating the heavy quark as static avoids this problem, and gives us the meson properties in the leading order in heavy-quark effective theories (expansions in 1/mQ). The results can then be extrapolated or interpolated to $m_Q = m_b$.

The paths P_t we use in our work are specific combinations of a product of fuzzed links in a straight line of length l. The rotations of the meson state are given by the representations of O_h: since we are working on the lattice, we have to restrict the SU(2) representations to the rotations allowed by the cubic symmetry and classify them under O_h. The representations (tabulated to L=4) are:

$$\begin{aligned}
&\mathrm{L} = 0 \quad A_1 \\
&\mathrm{L} = 1 \quad T_1 \\
&\mathrm{L} = 2 \quad E \ T_2 \\
&\mathrm{L} = 3 \quad A_2 \ T_1 \ T_2 \\
&\mathrm{L} = 4 \quad A_1 \ E \ T_1 \ T_2
\end{aligned}$$

For example, if we want to extract, say, the energy of an L=3 excited state, we should construct a path that is in the A_2 representation.

To be more explicit, let us define the sum of two paths in direction i as $s_i = pl_{i+} + pl_{i-}$, and the difference of the paths as $p_i = pl_{i+} - pl_{i-}$. Here pl_{i+} and pl_{i-} are the paths, straight lines of length l, in the positive and negative direction i, respectively. Note that the p_i are in the T_1 representation. The combinations appropriate for the discrete group of cubic rotations are then the A_1 symmetric sum $S = s_1 + s_2 + s_3$ and the E combinations of b_i which can be taken as $E(b_i) = (b_1 - b_2)$ and $(2b_3 - b_1 - b_2)/\sqrt{3}$. The b_i are different for different states: $\gamma_i p_i$ (no sum on i) for the P_+ operator, and s_i for the D_{+-} operator, for example.

The appropriate operators for static-light mesons are then

$$\mathrm{S} : \bar{Q}\gamma_5 Sq \text{ or } \bar{Q}\gamma_i Sq \tag{3.7}$$

$$\mathrm{P}_- : \bar{Q}1q \text{ or } \sum_i \bar{Q}\gamma_i p_i q \tag{3.8}$$

$$\mathrm{P}_+ : \bar{Q}E(\gamma_i p_i)q \quad \text{(no sum on } i\text{)} \tag{3.9}$$

$$\mathrm{D}_{+-} : \bar{Q}\gamma_5 E(s_i)q. \tag{3.10}$$

Note that the D_{+-} operator gives an unknown mixture of the D wave states D_- and D_+, since it does not probe the spin of the state.

The straight line paths are not enough, if one wants to study higher excited states. Following [31], we consider L-shaped paths P_t to access the D_- and D_+ states. We take each side of the L-shape to have the same length. Taking linear combinations of these we can now form paths in the T_2 representation (paths t_i where i is the direction normal to the plane of paths) and in the A_2 representation (paths h). The paths h are constructed by taking the sum with alternating sign of paths to the 8 corners of a spatial cube from the centre. The path to each corner of the cube is a sum of the six shortest routes along the axes from the centre of the cube to the corner, which then has to be projected onto the SU(3) group.

We now have operators in the T_2 representation, which allows us to separate the D_-, D_+ states since

$$\mathrm{D}_- : \bar{Q}E(\gamma_i t_i)q \quad \text{(no sum on } i\text{)} \tag{3.11}$$

and

$$\mathrm{D}_+ : \bar{Q}\sum_i (\gamma_i t_i)q. \tag{3.12}$$

We can also extract some information of the F-wave states, since the operator

$$\mathrm{F}_{+-} : \bar{Q}\gamma_5 hq \tag{3.13}$$

gives an L = 3, 6, ... state. This operator does not fix the spin of the light quark, and gives a mixture of both F-wave states, F_- and F_+.

The energies (m_i) and amplitudes (a_i) are extracted by fitting the C_2 with a sum of exponentials,

$$[C_2(T)]_{f_1,f_2} \approx \sum_{i=1}^{N_{\max}} a_{i,f_1} \mathrm{e}^{-m_i T} a_{i,f_2}, \text{ where } N_{\max} = 2 - 4,\ T \leq 14. \tag{3.14}$$

The fit is a simple least squares fit. In most of the cases 3 exponentials are used to try to ensure the first radially excited states are not polluted by higher states. Also 2 and 4 exponential fits are used to cross-check the results wherever possible. Two different levels of fuzzing (2 and 8 iterations of conventional fuzzing) are used in the spatial directions to permit a cleaner extraction of the excited states — see Eq. (2.16). We set $b_1 = 2.5$ and $b_2 = 1$ — the values used by UKQCD Collaboration earlier. Indices f_1 and f_2 denote the amount of fuzzing used at the vertices and both of them take two values, f_1 =F1, F2 and f_2 =F1, F2, where (F1=2 iterations and F2=2+6 iterations). For S and P_- states we have alternative operators (see [27]), so in all we get a 5 by 5 matrix (5 paths, because one operator has two choices, F1 and F2, and the other operator has three choices, local, F1 and F2) instead of just a 2 by 2 matrix (2 paths) given by the fuzzing choices. Here "local" means the original, unfuzzed link.

3.2 Smeared heavy quarks

In most of the study we use a "plain" heavy quark, i.e. the original Eichten–Hill point static source construction without smearing. However, especially in the excited state radial distribution measurements, the signal gets easily overcome by the noise. To get a better noise to signal ratio we introduce two types of smearing in the time direction: APE smearing and hypercubic blocking. The effect of smearing is studied in [4].

In APE smearing the original links in the time direction are replaced by a sum over the six staples that extend one lattice spacing in the spatial directions (in Fig. 3.2 on the left). This smearing is called here "sum6" for short.

To smear the heavy quark even more we also use hypercubic blocking (called here "hyp" for short). The smearing was first introduced by Hasenfratz and Knechtli in [32]. Here we again use smearing only for the links in the time direction, as in the "sum6" smearing above. A schematic picture of hypercubic blocking is in Fig. 3.2 on the right. In "hyp" the staples (the red dashed lines in Fig. 3.2) are not constructed from the original, single links, but from staples (the blue dash-dotted lines in Fig. 3.2). Hypercubic blocking takes

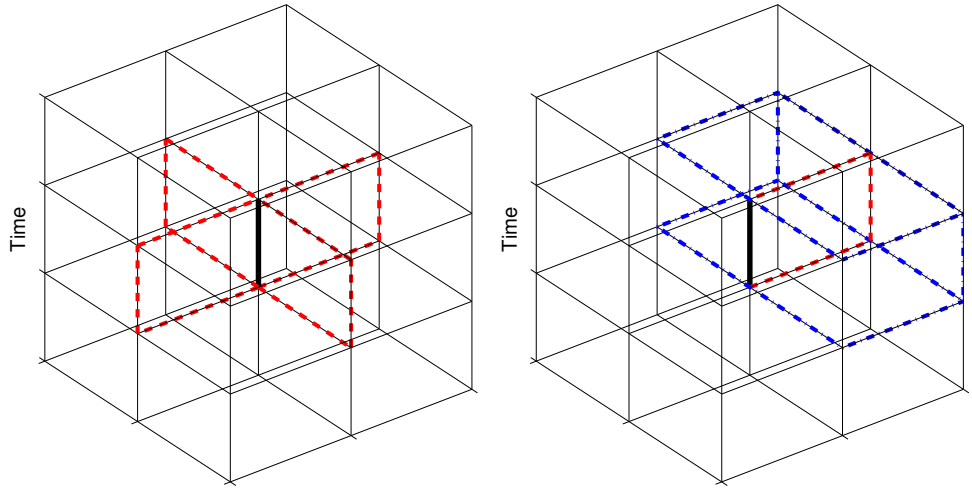

Figure 3.2: (Colour online) APE smearing in the time direction (on the left) and hypercubic blocking (on the right). In both cases the original, unsmeared basic link is replaced by the solid black link (a combination of neighbouring links as explained in the text).

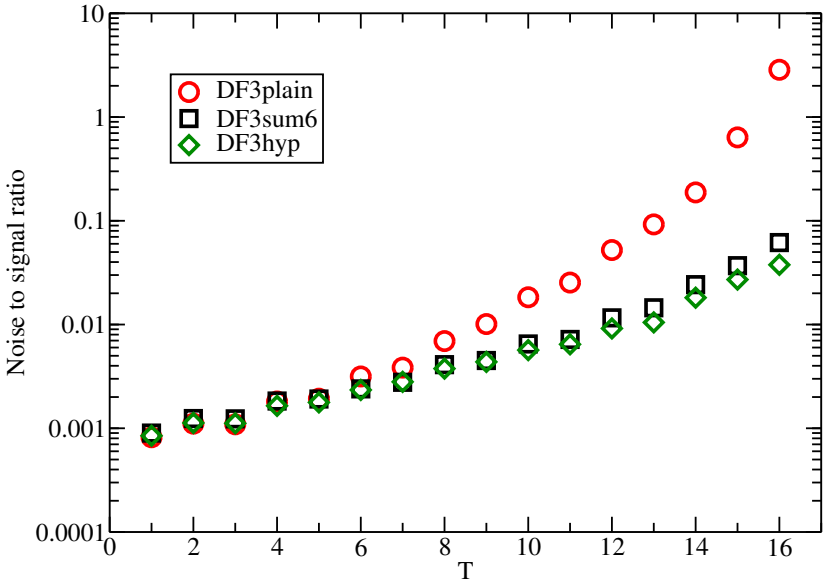

Figure 3.3: (Colour online) Noise (standard deviation) to signal ratio: S wave 2-point correlation function C_2 for the lattice "DF3". Note the logarithmic scale.

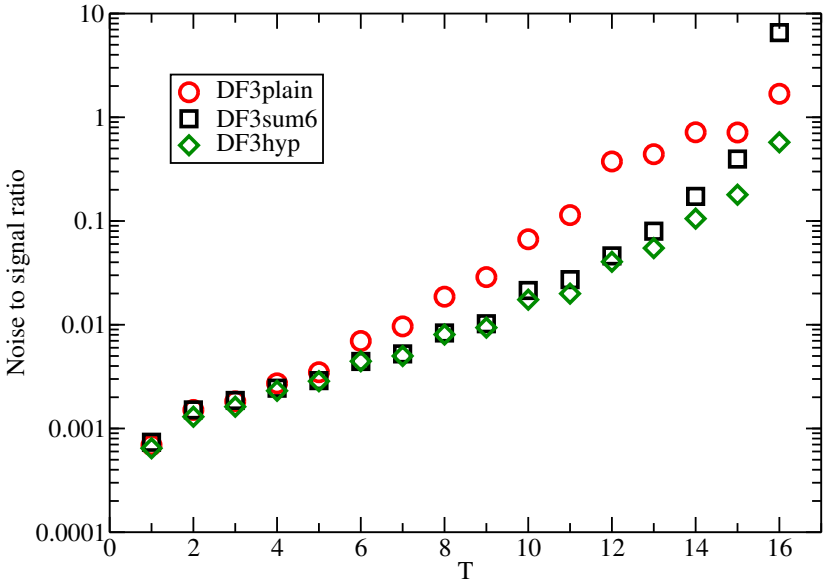

Figure 3.4: (Colour online) Noise (standard deviation) to signal ratio as in Fig. 3.3 but for the P_- case.

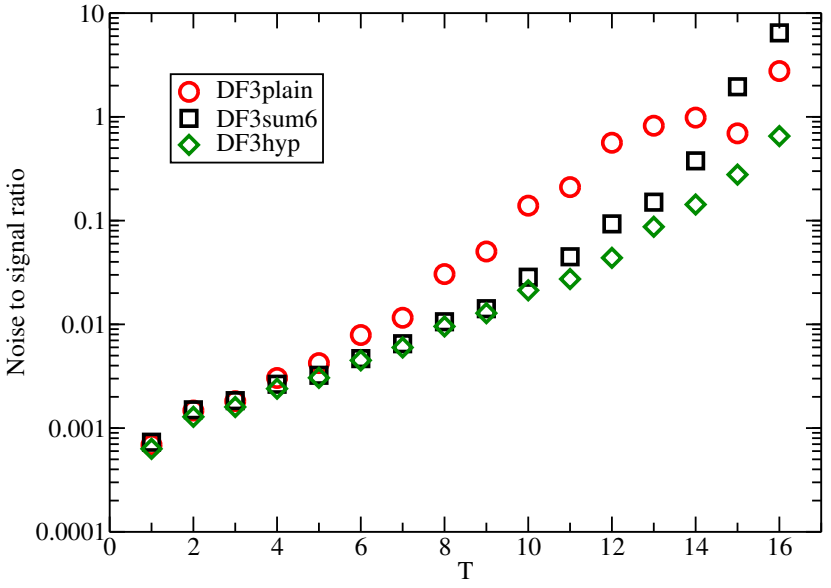

Figure 3.5: (Colour online) Noise (standard deviation) to signal ratio for the P_+ case.

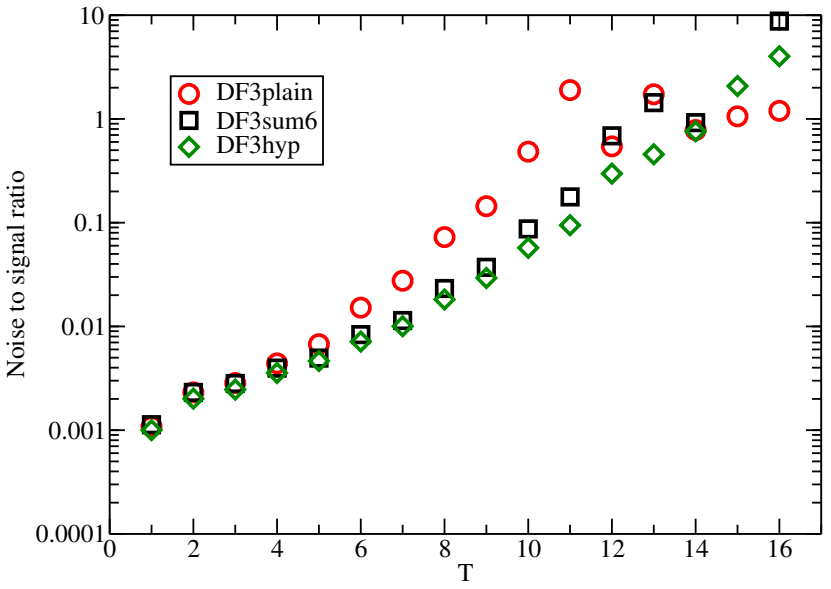

Figure 3.6: (Colour online) Noise (standard deviation) to signal ratio for the D_- case.

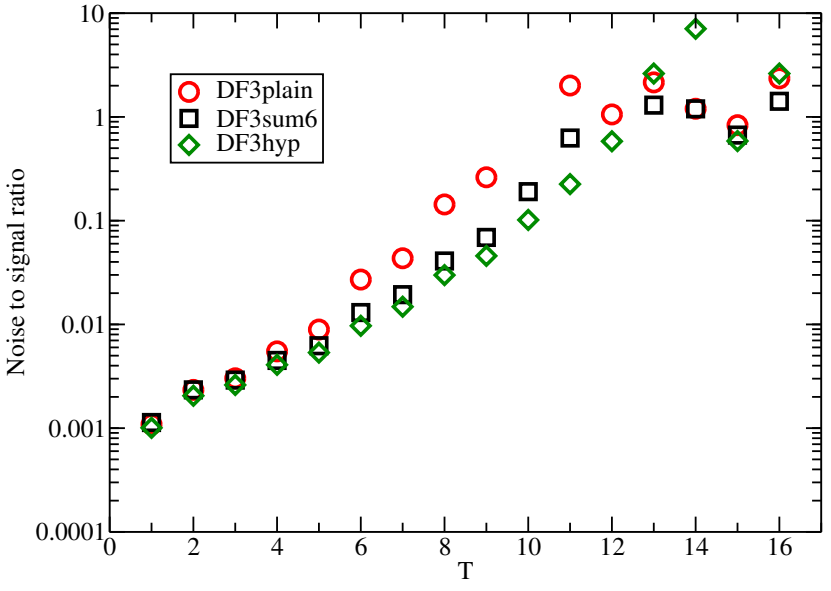

Figure 3.7: (Colour online) Noise (standard deviation) to signal ratio for the D_+ case.

into account the links within a "hypercube" (the edges of the "cube" are $2a$ in spatial directions but only one lattice spacing in the time direction).

In analogy with the fuzzing described in Chapter 2 [Eq. (2.16)], we first construct the links

$$\bar{V}_{i,\mu;\nu\rho} = \mathrm{Proj}_{\mathrm{SU(3)}}\left[(1-\alpha_3)U_{i,\mu} + \frac{\alpha_3}{2}\sum_{\pm\eta\neq\rho,\nu,\mu} U_{i,\eta}U_{i+\hat{\eta},\mu}U^{\dagger}_{i+\hat{\mu},\eta}\right], \tag{3.15}$$

where $U_{i,\mu}$ is the original thin link at location i and direction μ. There are no staples in directions ν or ρ — hence the notation $\bar{V}_{i,\mu;\nu\rho}$. We then construct "fat" links

$$\tilde{V}_{i,\mu;\nu} = \mathrm{Proj}_{\mathrm{SU(3)}}\left[(1-\alpha_2)U_{i,\mu} + \frac{\alpha_2}{4}\sum_{\pm\rho\neq\nu,\mu} \bar{V}_{i,\rho;\nu\mu}\bar{V}_{i+\hat{\rho},\mu;\rho\nu}\bar{V}^{\dagger}_{i+\hat{\mu},\rho;\nu\mu}\right], \tag{3.16}$$

where index ν indicates that the link is not decorated with staples in that direction. The last step is

$$V_{i,\mu} = \mathrm{Proj}_{\mathrm{SU(3)}}\left[(1-\alpha_1)U_{i,\mu} + \frac{\alpha_1}{6}\sum_{\pm\nu\neq\mu} \tilde{V}_{i,\nu;\mu}\tilde{V}_{i+\hat{\nu},\mu;\nu}\tilde{V}^{\dagger}_{i+\hat{\mu},\nu;\mu}\right], \tag{3.17}$$

where the "fat" links are again used to construct the new links. Here, as for "sum6", we only consider $V_{i,\mu}$ with μ in the time direction, and use conventional fuzzing for the spatial directions. The coefficients α_1, α_2, α_3 can be tuned to get maximal benefit of the hypercubic blocking. In our study we use $\alpha_3 = 0.5$, $\alpha_2 = 1$ and $\alpha_1 = 1$, because this choice was found to be very good in reducing the noise to signal ratio in [33]. Note that $\alpha_3 = 1$, $\alpha_2 = 0$ and $\alpha_1 = 0$ would give the "sum6" smearing.

Smearing the heavy quark really does improve the noise to signal ratio, as can be seen in Figs. 3.3–3.7. We only considered smearing the heavy quark in the latest measurements, that were done with dynamical fermions. The figures show the standard deviation to signal ratio for the largest component of C_2, which is F2F2, for 160 lattice configurations (lattice "DF3"). In all cases the "plain" signal is clearly inferior to the "sum6" and "hyp" signals, whereas the "hyp" signal is also somewhat better than the "sum6" signal for the larger values of T. This latter difference would be more apparent in a non-logarithmic scale. Lattices "DF4" and "DF5" show similar trends as the "DF3" lattice.

3.3 The lattice results

The extracted energies can be considered from different viewpoints. Firstly Fig. 3.8 shows the resulting energy spectrum for the lattice "DF3" as an example. The energies are from the fit in Equation (3.14). We can only look at energy differences due to the unknown

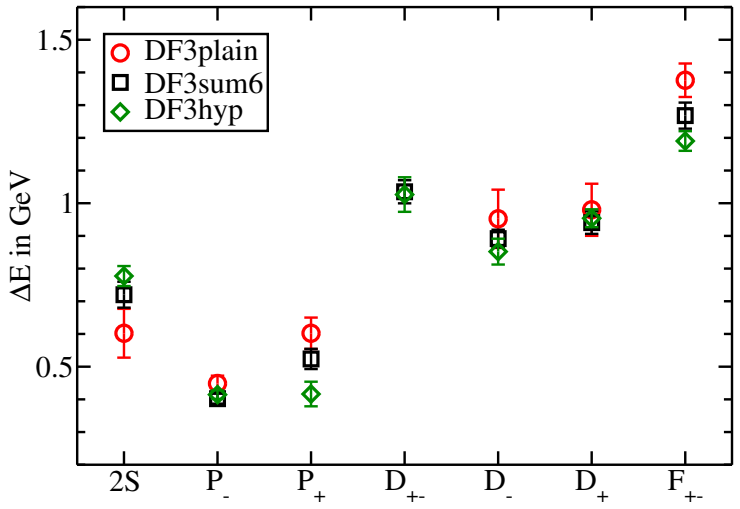

Figure 3.8: (Colour online) Energy spectrum of the heavy-light meson using lattice "DF3". Here L_+ (L_-) means that the light quark spin couples to angular momentum L giving the total $j = L + 1/2$ ($j = L - 1/2$). The 2S is the first radially excited L= 0 state. The D_{+-} is a mixture of the D_- and D_+ states, and likewise for the F_{+-}. Energies are given with respect to the S wave ground state (1S). Here $r_0/a = 4.754(40)^{+2}_{-90}$ (from [29]) and $r_0 = 0.525$ fm were used to convert the energy differences to physical units. The error bars shown here contain only the statistical errors on the lattice energy fits.

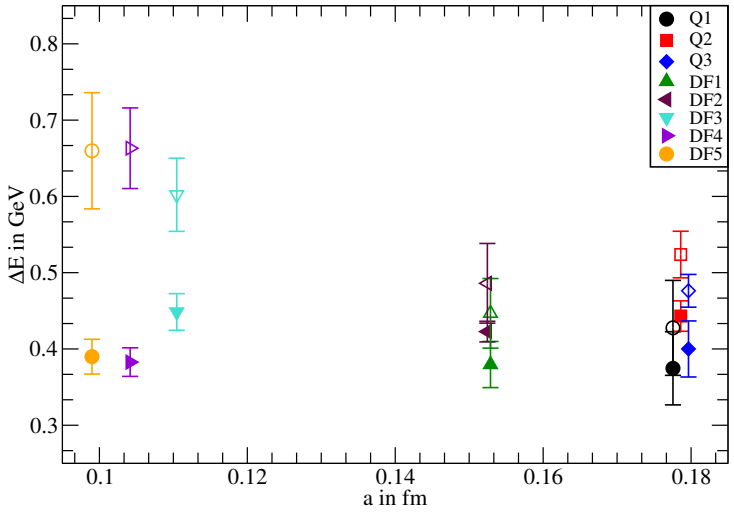

Figure 3.9: (Colour online) Energies of the two P wave states, $[E(P_-) - E(1S)]$ (filled symbols) and $[E(P_+) - E(1S)]$ (open symbols) as a function of the lattice spacing a. Here $r_0 = 0.525$ fm was used to convert the energy differences to physical units. These results are from "plain" measurements, i.e. no smearing in the time direction.

self energy that is a constant for a given lattice for all L values and radial excitations. Hence we give the energies with respect to the lowest energy 1S. Here we also compare the different smearings: "plain", "sum6" and "hyp". Our preferred smearing is "hyp", because — in addition to being the most refined — it has the best signal to noise ratio, with "sum6" as a close second (see [4] for more details). For some states, particularly the P_- and D_+ states, all smearings give the same energy differences, but the "plain" results have larger errors than the other two. However, the differences in the results between the three smearings can be large, as can be seen for the P_+ state. This is probably due to the lattice spacing a being too far away from zero — it should be noted that the results for the different smearings only need to agree in the continuum limit.

A second way to present the results is in Figs. 3.9 and 3.10, where we compare our results from different lattices. All lattices use the "plain" configurations, i.e. no smearing in the time direction, to compare like with like. On one hand, we can now compare quenched and unquenched results. On the other hand, this plot can be used to check how much the results change when the lattice spacing a changes, although for a proper continuum extrapolation the lattices should be similar (aside from the lattice spacing). The quenched results ("Q1", "Q2", "Q3", from [3]) are rather similar to those unquenched

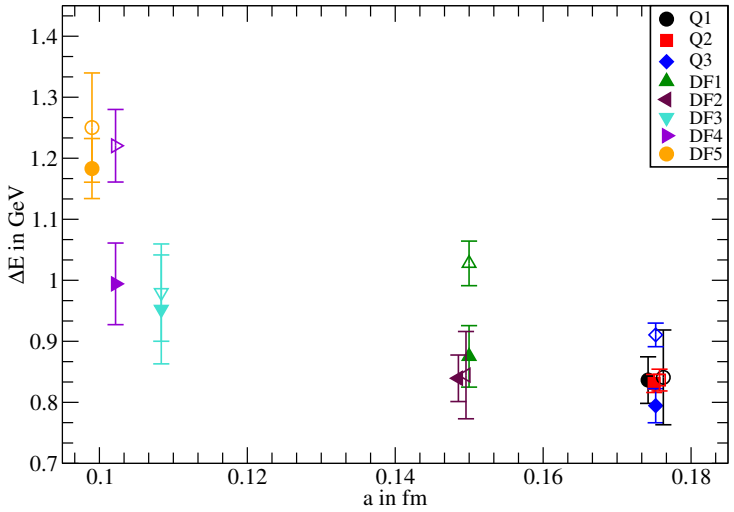

Figure 3.10: (Colour online) Energies of the two D wave states, $[E(D_-) - E(1S)]$ (filled symbols) and $[E(D_+) - E(1S)]$ (open symbols) as a function of the lattice spacing a. Here $r_0 = 0.525$ fm was used to convert the energy differences to physical units. These results are from "plain" measurements, i.e. no smearing in the time direction.

results ("DF1", "DF2", both "plain", from [3]) that have larger lattice spacings (about 0.15 fm), but the unquenched lattices with smaller lattice spacings ($a \approx$0.10–0.12 fm, i.e. lattices "DF3", "DF4" and "DF5", all "plain", from [3] and [4]) give higher energy differences $E(P_+) - E(1S)$, $E(D_-) - E(1S)$ and $E(D_+) - E(1S)$. All lattices should, of course, give the same result in the continuum limit, but at a fixed, non-zero a the results may differ considerably. To draw any definite conclusions smaller errors and a reliable extrapolation to the continuum limit would be needed.

A third way to present the results is to check how they depend on the light quark mass. To do this we plot the energies (i.e. energy differences with respect to the 1S state) as a function of the pion mass squared, $(m_\pi)^2$ — see Table 3.2. Figs. 3.11–3.16 show that P and D wave state energies (using lattices "DF3", "DF4" and "DF5" with smearing) do not depend strongly on the light quark mass, although some dependence can be seen. In most cases the errors are too large to make definitive conclusions. It is also interesting to compare our results with twisted mass lattice calculations from [34] (European Twisted Mass Collaboration). The results agree fairly well, except for the P_- and $F_\pm$ states. This can be, for example, due to different $\mathcal{O}(a^2)$ effects.

We also compare our results to other static-light meson lattice calculations in Fig. 3.17.

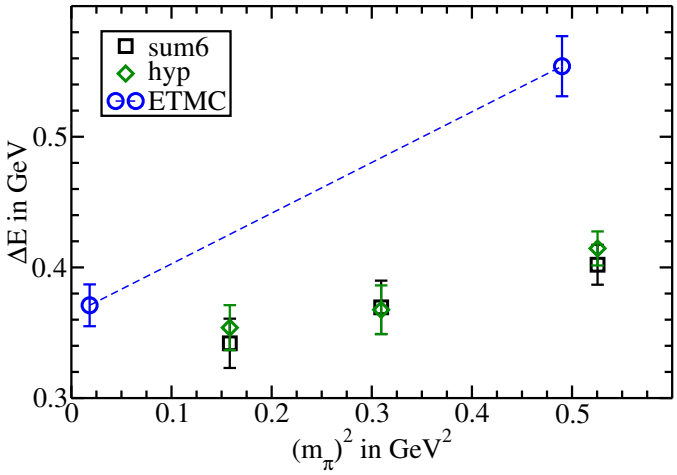

Figure 3.11: (Colour online) The energy difference $[E(1P_-) - E(1S)]$ as a function of the pion mass squared. Our results show only a slight dependence on the light quark mass. Here and in the following figures for P_+, D_-, D_+, $F_\pm$ and 2S the "sum6" and "hyp" results, from left to right, are from lattices "DF5", "DF4" and "DF3", respectively. The European Twisted Mass Collaboration's results (ETMC) are from [34].

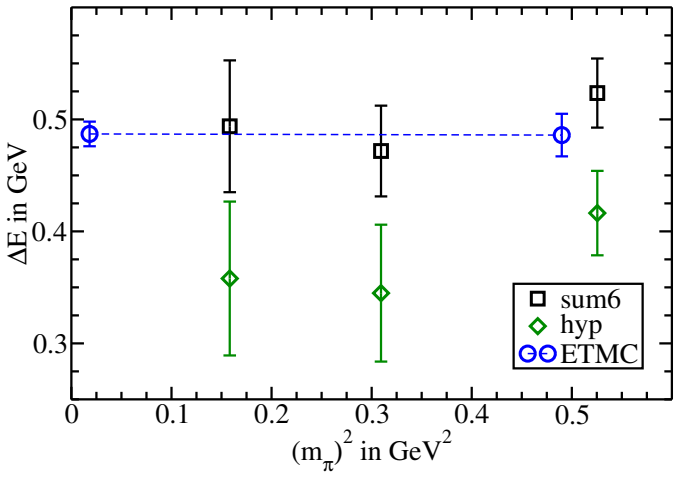

Figure 3.12: (Colour online) The energy difference $[E(1P_+) - E(1S)]$ as a function of the pion mass squared. The European Twisted Mass Collaboration's results (ETMC) are from [34].

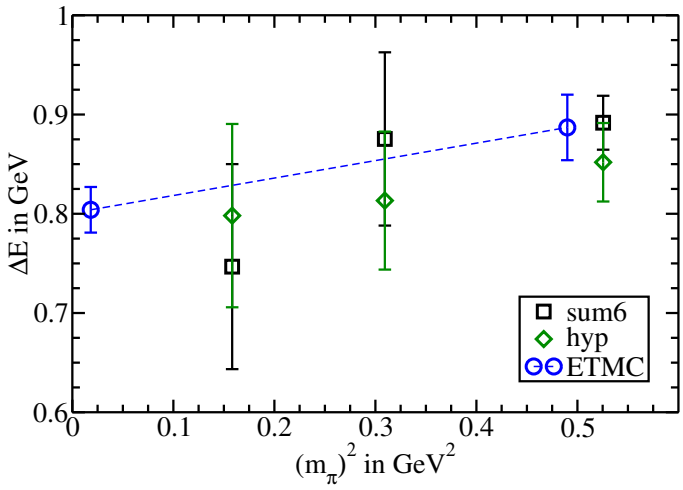

Figure 3.13: (Colour online) The energy difference [E(1D$_-$) − E(1S)] as a function of the pion mass squared. The European Twisted Mass Collaboration's results (ETMC) are the D$_\pm$ results from [34].

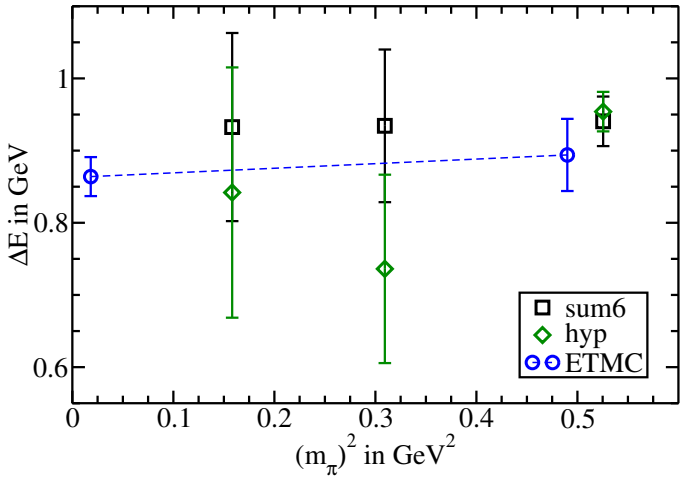

Figure 3.14: (Colour online) The energy difference [E(1D$_+$) − E(1S)] as a function of the pion mass squared. The European Twisted Mass Collaboration's results (ETMC) are from [34].

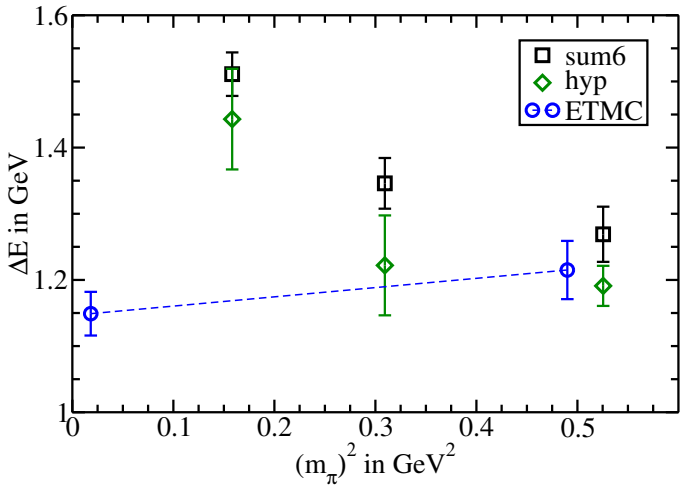

Figure 3.15: (Colour online) The energy difference $[E(1F_{\pm}) - E(1S)]$ as a function of the pion mass squared. The European Twisted Mass Collaboration's results (ETMC) are from [34].

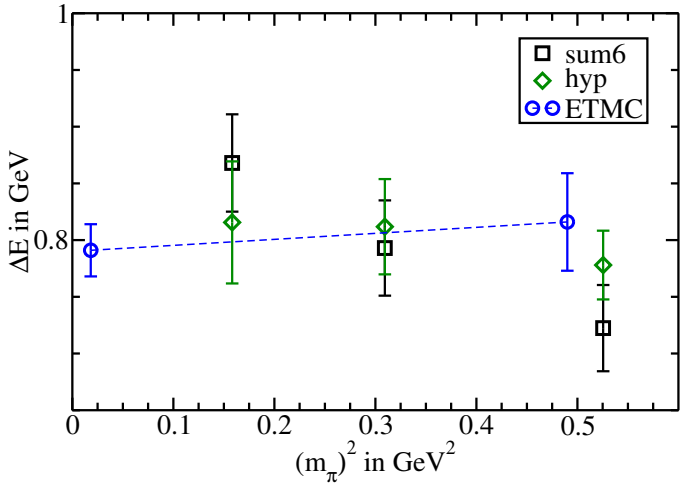

Figure 3.16: (Colour online) The energy difference $[E(2S) - E(1S)]$ as a function of the pion mass squared. The European Twisted Mass Collaboration's results (ETMC) are from [34].

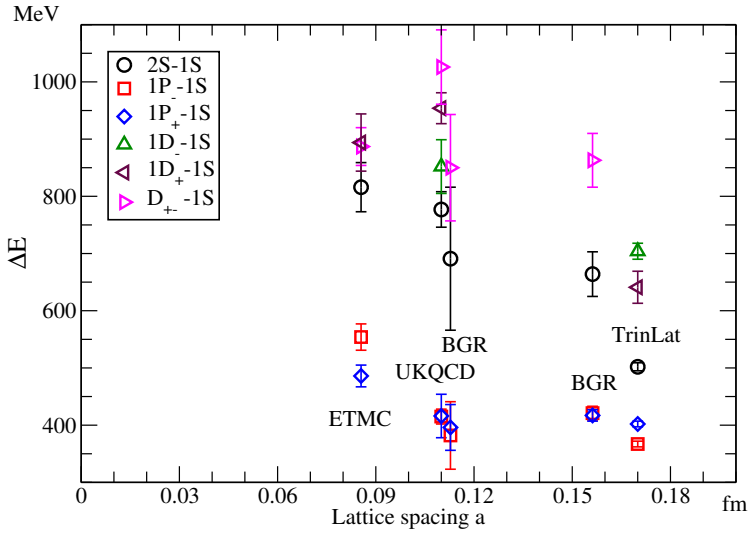

Figure 3.17: (Colour online) Comparison of different static-light lattice results. On the left at $a = 0.0855$ fm are the results from European Twisted Mass Collaboration [34], at $a = 0.11$ fm our "DF3hyp" results from [4], at $a = 0.113$ fm and $a = 0.156$ fm BGR Collaboration's results [35] and on the right at $a = 0.17$ fm TrinLat group's results [36, 37]. A set of similar lattices with different lattice spacings is needed for going to the continuum limit.

There it is seen that the P wave results do not change much between the different lattices (except for the ETMC results), but the $2\mathrm{S} - 1\mathrm{S}$ and D wave energy differences vary a lot. However, since the lattices and lattice spacings are different, the results should only agree in the continuum limit. A set of similar lattices with different lattice spacings would be needed to check this.

3.4 Interpolation to the b quark mass

Until now we have measured the two-point correlators on the lattice, and extracted the energies of several excited states of the static-light mesons. However, if we want to compare the lattice results to actual experimental results, we should try to predict where the B_s meson excited states lie. To obtain the predictions we can interpolate in $1/m_Q$, where m_Q is the heavy quark mass, between the static-light lattice calculations and D_s meson experimental results, i.e. interpolate between the static quark ($m_Q = \infty$) and the charm quark ($m_Q = m_c$). We should, of course, go to the continuum limit before doing

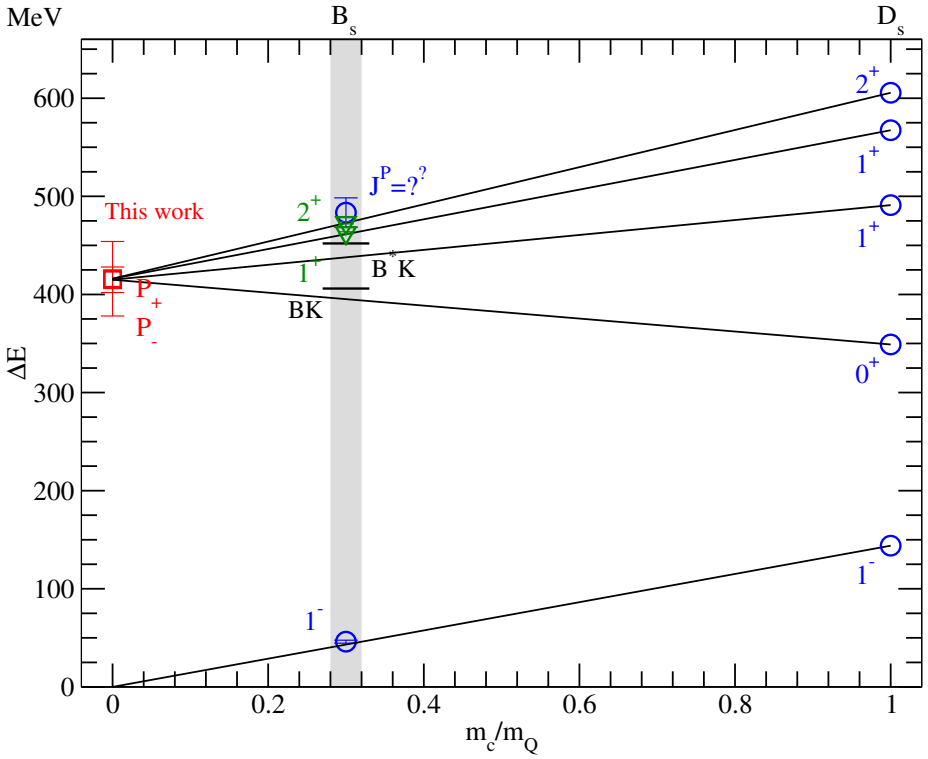

Figure 3.18: (Colour online) Interpolation to the b quark mass. The ratio m_c/m_b is taken to be 0.30(2) (from [5]; shown by the vertical band). The D_s meson experimental results are from [5] (blue circles), and the B_s meson experimental results are from [5] (blue circles) and [11, 12, 10] (green triangles). Our results (using "DF3hyp" configurations) are marked with red squares.

this, but due to the lack of suitable lattice configurations we have to settle for the fixed a results. We thus use the "DF3hyp" results for the static-light energies, as it is our most elaborate treatment of the system, and the light quark mass is close to the strange quark mass.

When doing the interpolation we have to assume that the measured D_s meson states are simple $Q\bar{q}$ states, like our lattice states are (except for the contribution from the dynamical fermions). This is not necessarily true: for example the mass of the $D^*_{s0}(2317, 0^+)$ is much lower than what is predicted by conventional potential models, and it has thus been proposed that it could be either a four quark state, a DK molecule or a $D\pi$ atom. This topic has been discussed a lot, and a short review on meson excited state spectroscopy and the puzzles in interpreting the results is given for example in Ref. [38]. However, in [39] Lee and Lee suggested that the inclusion of chiral radiative corrections could change the potential model predictions considerably. In the following we assume that the states are the usual $Q\bar{q}$ states.

As explained in [4] we use linear interpolation, i.e.

$$\Delta E = A + B\frac{m_c}{m_Q} + CF_j\frac{m_c}{m_Q}\,. \tag{3.18}$$

The coefficient $F_j = 2[J(J+1) - j_q(j_q+1) - s_Q(s_Q+1)]$, where J is the total angular momentum, $s_Q = 1/2$ is the heavy quark spin and j_q is the combined spin and orbital angular momentum L of the light quark (see Table 3.3). (At the beginning of Section 3.1, the notation $j = j_q$ was used.) Constants A, B and C are fixed by fitting three data points, for example the P$_-$ lattice result (this fixes A, as $m_c/m_Q = 0$) and the two lowest D_s meson P wave states 0^+ and 1^+ (experimental results). The interpolation procedure is shown in Fig. 3.18. It should be noted that this linear interpolation works perfectly for the 1^- S wave state, where the experimental energies are known for both B_s and D_s mesons. The lattice result for this state is zero, because the two 1S states ($J^P = 0^-$, 1^-) are automatically degenerate at $m_Q = \infty$. Note that we have to subtract the energy of the lowest S wave state (0^-), as we have the unknown self energy in the lattice results.

Our predictions of the energy differences $m(1P) - m(1S)$ for the B_s meson are given in Table 3.4. For our preferred lattice "DF3hyp" these agree very well with the experimental measurements of the energies of the 1^+ and 2^+ P wave states. Also we predict that the two lowest P wave states (0^+, 1^+) lie a few MeV below the BK and B^*K thresholds (minus the 1S state energy) at 406 and 452 MeV respectively. We show the "DF3sum6" results for comparison.

To compare with other lattice calculations, we can plot the heavy-light meson lattice results as a function of $1/m_Q$. In Fig. 3.19 we show the P wave and 2S lattice results from

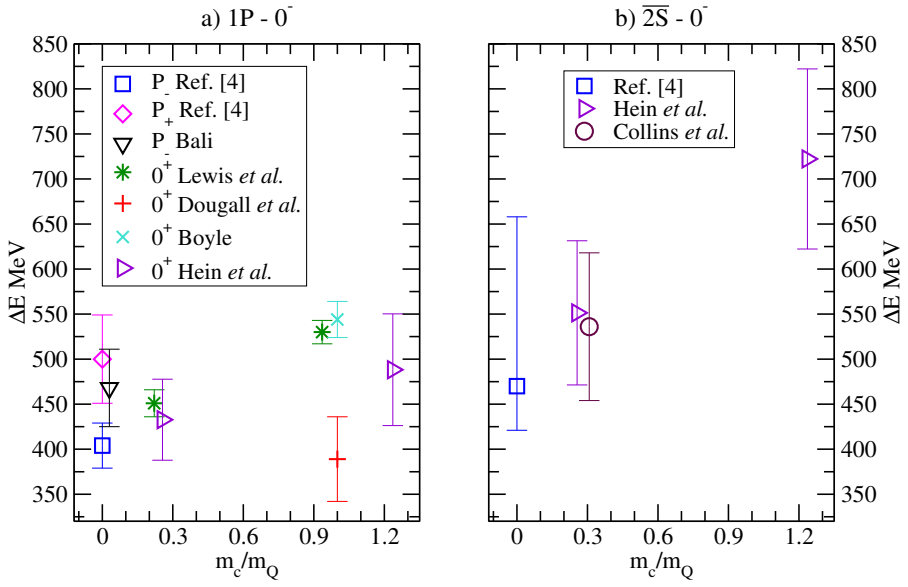

Figure 3.19: (Colour online) The energies from various lattice studies of heavy-light excited states relative to the ground state ($J^P = 0^-$) heavy-light meson with a heavy quark of mass m_Q and light quark which is strange (i.e. $Q\bar{s}$ mesons). For clarity we have displaced some of the numbers on the x axis. The graph should be viewed as three clumps of numbers with heavy quarks at static, bottom (B_s) and charm (D_s). The results are from [3] (our work), [40] (Bali), [41] (Lewis *et al.*), [42] (Dougall *et al.*), [43] (Boyle), [44] (Hein *et al.*) and [45] (Collins *et al.*).

J^P	L	F_j	J^P	L	F_j	J^P	L	F_j
0^+	0	-3	0^+	1	-3	1^+	1	-5
1^+	0	$+1$	1^+	1	$+1$	2^+	1	$+3$

Table 3.3: Coefficients $F_j = 2[J(J+1) - j_q(j_q+1) - s_Q(s_Q+1)]$ (equation (3.18)).

J^P	DF3hyp	DF3sum6	experiments
0^+	393 ± 9 MeV	384 ± 10 MeV	-
1^+	440 ± 9 MeV	432 ± 10 MeV	-
1^+	466 ± 25 MeV	538 ± 21 MeV	463 ± 1 MeV
2^+	482 ± 25 MeV	551 ± 21 MeV	473 ± 1 MeV

Table 3.4: Our predictions for B_s meson mass differences, m(B_s^*)-m(B_s), for the P wave states. The uncertainty in the ratio m_c/m_b is not taken into account in the error estimates. The experimental results are from [10, 11, 12].

various studies: At $m_c/m_Q = 0$ we have the static heavy quark results, at $m_c/m_Q \approx 0.3$ the heavy quark is close to a b quark (B_s meson) and at $m_c/m_Q = 1$ the heavy quark is a c quark (D_s meson). This Figure can be compared with Fig. 3.18, where we use experimental results to do the extrapolation. The experimental results for the two lowest P wave state of the D_s meson are $m(0^+) - m(0^-) = 349$ MeV and $m(1^+) - m(0^-) = 491$ MeV, whereas the $m_Q \approx m_c$ lattice calculations give results in the range 375–575 MeV for $m(0^+) - m(0^-)$.

Higher excitations can be extrapolated to $m_Q = m_b$ in the same way as the P wave states, if the energies of the corresponding D_s meson states are known from experiments. There is some experimental input available, as BaBar and Belle observed two new states, $D_{sJ}^*(2860)$ and $D_{sJ}^*(2700)$, in 2006 [7, 8, 9]. Unfortunately it is not clear what the quantum numbers of these states are. The $D_{sJ}^*(2860)$ quantum numbers can be $J^P = 0^+$, 1^-, 2^+, etc., so it could be a radial excitation of the $D_{s0}^*(2317)$ or a $J^P = 3^-$ D wave state. The first interpretation is rather popular, but our lattice results favor the D wave $J^P = 3^-$ assignment in agreement with Colangelo, De Fazio and Nicotri [46]. If this latter assignment is assumed, the interpolation predicts the energy difference of the 3^- D wave B_s meson state and the S wave ground state to be 932(18) MeV (see Fig. 3.20). Assigning the $D_{sJ}^*(2860)$ as a radial excitation of the $D_{s0}^*(2317)$ does not seem as natural, as the slope of the interpolating line would be very steep. The second one of the measured excited states, the $D_{sJ}^*(2700)$, could be a radially excited S wave state or a D wave $J^P = 1^-$ state. If we assume the latter identification, then a D wave $J^P = 1^-$ B_s meson state is predicted

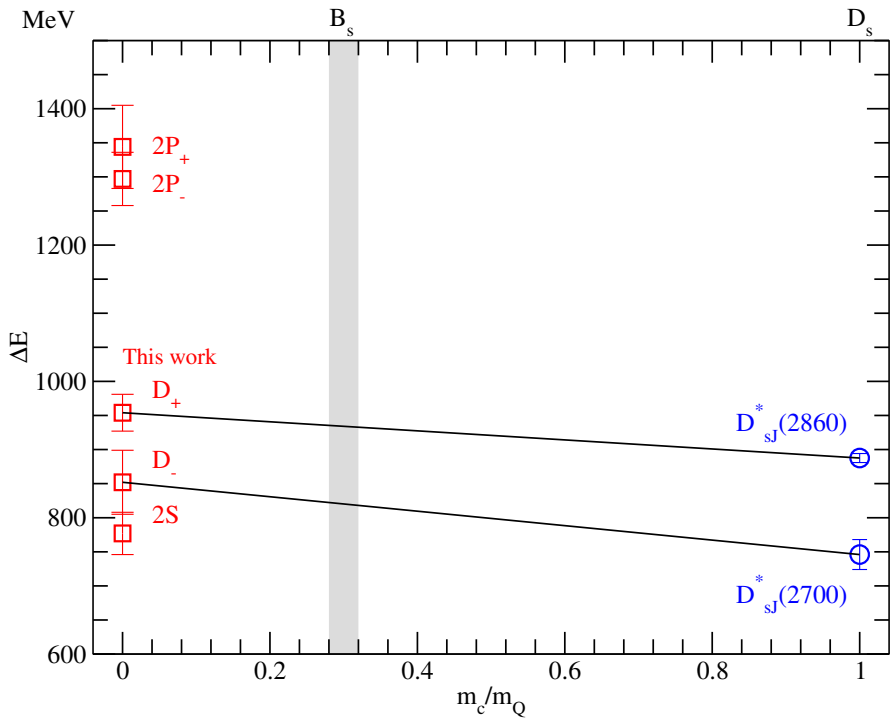

Figure 3.20: (Colour online) Interpolation to the b quark mass for the "DF3hyp" lattice: higher excited states. The lines illustrate what the interpolation would look like, assuming the D_s meson states were D wave states. The experimental results are from [7, 8, 9]. Interpolating to m_c/m_b predicts D wave $J^P = 1^-$, 3^- at 817(31) and 932(18) MeV respectively.

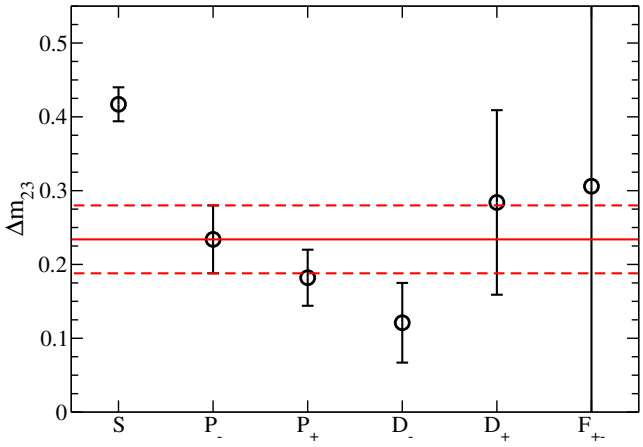

Figure 3.21: (Colour online) Mass differences $\Delta m_{32} = m_3 - m_2$ for the "DF3hyp" data in lattice units. This seems to be essentially constant for angular momentum L$\geq$ 1 (given the sizeable errors on the data). The lines give the $\Delta m_{32} = 0.234(46)$ that is used in this study. Looking at the "DF3sum6" data gives a very similar picture (not shown here) and an estimate of $\Delta m_{32} = 0.207(54)$. See section 3.5 for details.

to lie 817(31) MeV above the 1S state (also shown in Fig. 3.20).

3.5 Bayesian inspired analysis

All energies are extracted using the fit in Eq. (3.14). We would like to use 3 exponentials to fit the C_2 data to ensure the ground state and first excited state energies are not polluted by the higher excited states. However, using 3 exponentials requires many fit parameters, and the fits do not work very well in all cases. This is especially a problem for some D and F wave states with those lattice configurations, where the signal is not strong enough. Using only 2 exponentials in the fit would of course be one option, but one can keep the third exponential by introducing some Bayesian ideas and using prior knowledge of the energies to constrain the fit. Restricting the third energy in the fit to a certain range guides the fit in the right direction and makes the fit more stable. This improvement in the data analysis is introduced in [4].

The third mass, m_3, would be the mass of the second radial excitation, if there was no pollution from higher states. If the 3 exponential fit is unstable, we restrict the m_3 to be

$nL_{\pm}$	m_3 3 exp	$m_{3,\text{ prior}}$	m_3 Bayes	m_2 3 exp	m_2 Bayes
P_+	1.46(2)	1.52(6)	1.471(15)	1.28(3)	1.29(3)
D_-	1.63(5)	1.74(6)	1.67(4)	1.51(3)	1.52(2)
D_+	1.84(12)	1.79(5)	1.80(2)	1.559(11)	1.558(8)
F_{+-}	1.96(43)	1.89(5)	1.89(1)	1.66(2)	1.657(5)

Table 3.5: Comparison of the $m_{3,\text{prior}}$ with the results from the full 3 exponential fit and the Bayesian fit for "DF3hyp" configurations. See Section 3.5 for definition of $m_{3,\text{prior}}$. Here "m_3 3 exp" and "m_3 Bayes" are the results of a full 3 exponential fit and a Bayesian (fixed m_{32}) fit, respectively — likewise for the m_2. The P_+ "Bayes" fit is merely to check that the Bayesian ideas work well and does not restrict the analysis too much.

$nL_{\pm}$	m_3 3 exp	$m_{3,\text{ prior}}$	m_3 Bayes	m_2 3 exp	m_2 Bayes
P_+	1.59(2)	1.61(5)	1.59(2)	1.39(2)	1.393(15)
D_-	1.80(9)	1.79(5)	1.79(3)	1.578(11)	1.577(8)
D_+	2.1(2)	1.82(5)	1.84(2)	1.604(12)	1.596(11)
F_{+-}	2.6(9)	1.94(6)	1.950(11)	1.72(2)	1.721(8)

Table 3.6: Comparison of the $m_{3,\text{prior}}$ with the results from the full 3 exponential fit and the Bayesian fit for "DF3sum6" configurations. Again, the prior m_3 values are in fairly good agreement with the m_3 results from the full 3 exponential fits. Fixing $m_3 - m_2$ does not change the first excited state m_2. See Table 3.5 for notation.

in the range $m_{3,\text{ prior}} \pm \Delta m_{3,\text{ prior}}$ by adding a term

$$\frac{(m_3 - m_{3,\text{ prior}})^2}{(\Delta m_{3,\text{ prior}})^2} \tag{3.19}$$

to the χ^2. Unlike fixing m_3 to a given value, this is not a very strict constraint, since it only softly limits the parameter to a given range. The values of $m_{3,\text{ prior}}$ and $\Delta m_{3,\text{ prior}}$ have to be determined beforehand. We choose to determine these prior values by estimating the difference $\Delta m_{32} = m_3 - m_2$ from full 3 exponential fits. This mass difference seems to be almost constant for states that have $L = 1$ or higher, as can be seen in Fig. 3.21. Therefore we use the P_- state to set the Δm_{32} for D wave and F wave states. The $m_{3,\text{ prior}}$ for D wave and F-wave states is then calculated by adding Δm_{32} to the m_2 from the full 3 exponential fit for the state in question (see Tables 3.5, 3.6). The prior m_3 values are in fairly good agreement with the m_3 results from the full 3 exponential fits, and fixing $m_3 - m_2$ does not change the first excited state m_2. The P_+ "Bayes" fit are used to check that the Bayesian ideas work well and does not restrict the analysis too much.

3.6 Spin-orbit splitting

The spin-orbit splitting, $E(L_+) - E(L_-)$, and the order of the states in a spin multiplet are of great interest, as that can tell us something about the interaction between quarks. In a Coulombic spectrum the L_+ state lies higher than the L_-, whereas the multiplets should become more and more inverted as L increases if a pure scalar confining potential is present [47, 48]. Experimentally this inversion is not seen for P wave mesons, and lattice measurements are now used to study whether the inversion could be seen in the D wave multiplet.

We extract this energy difference of the $1P_+$ and $1P_-$ states in two different ways:

1. *Indirectly* by simply calculating the difference using the energies given by the fits in Eq. (3.14), when the P_+ and P_- data are fitted separately.

2. Combining the P_+ and P_- data and fitting the ratio $C_2(P_+)/C_2(P_-)$, which enables us to go *directly* for the spin-orbit splitting, $m(1P_+) - m(1P_-)$.

In the latter case, the expression (for a given fuzzing) is

$$\frac{C_2(P_+)}{C_2(P_-)} = A\, e^{-\Delta m_1 T}\left[\frac{1 + b_2^+\, e^{-\Delta m_2^+ T} + b_3^+\, e^{-\Delta m_3^+ T}}{1 + b_2^-\, e^{-\Delta m_2^- T} + b_3^-\, e^{-\Delta m_3^- T}}\right], \tag{3.20}$$

where

$$\begin{aligned}
\Delta m_1 &= m(1\mathrm{P}_+) - m(1\mathrm{P}_-)\,, \\
\Delta m_2^+ &= m(2\mathrm{P}_+) - m(1\mathrm{P}_+)\,, \\
\Delta m_2^- &= m(2\mathrm{P}_-) - m(1\mathrm{P}_-)\,, \\
\Delta m_3^+ &= m(3\mathrm{P}_+) - m(1\mathrm{P}_+) \text{ and} \\
\Delta m_3^- &= m(3\mathrm{P}_-) - m(1\mathrm{P}_-).
\end{aligned}$$

We get the best results by fitting the energy differences Δm_1, Δm_2^+, Δm_2^- and the coefficients A, b_2^+ and b_2^-, but fixing the Δm_3^+, Δm_3^- and the corresponding coefficients b_3^+, b_3^- from the individual two-point correlator fits (equation (3.14)). Thus

$$b_3^+ = \frac{a_{3,f_1}(\mathrm{P}_+)a_{3,f_2}(\mathrm{P}_+)}{a_{1,f_1}(\mathrm{P}_+)a_{1,f_2}(\mathrm{P}_+)} \text{ and } b_3^- = \frac{a_{3,f_1}(\mathrm{P}_-)a_{3,f_2}(\mathrm{P}_-)}{a_{1,f_1}(\mathrm{P}_-)a_{1,f_2}(\mathrm{P}_-)} \tag{3.21}$$

for given values of fuzzing indices f_1, f_2. The D wave spin-orbit splitting is also extracted in a similar manner.

Our most detailed study of the spin-orbit splitting is done with the dynamical lattices "DF3", "DF4" and "DF5". The results of the fits are given in Tables 3.7, 3.8 and in Figs. 3.22–3.27 (from [4]). One interesting point to note here is that the spin-orbit splitting of the P wave states is small, almost zero, for the preferred "hyp" smearing. The smearing affects the results a lot, as the P wave SOS is clearly positive and non-zero for "plain" and "sum6". This could be due to different $\mathcal{O}(a)$ effects. In all cases the errors on the direct estimates are much smaller than those on the indirect ones. Also in most cases the direct and indirect estimates are consistent with each other — the only exception being the P wave "sum6" estimates. There the direct value is somewhat lower than the indirect estimate and thus lending support to the most elaborate "hyp" estimate. The D wave spin-orbit splitting (SOS) results are more varied, but the "DF3hyp" lattice suggests clearly a positive, non-zero D wave SOS. However, the "DF4hyp" and "DF5hyp" estimates are considerably smaller, becoming negative for the "DF4hyp". At present it is not clear whether this is a lattice artifact due to, say, not being in the continuum limit, or that indeed the D wave results are more dependent on m_q than in the P wave case.

In contrast to our results, another lattice group finds the P wave SOS to be positive (about 35 MeV) and the D wave SOS to be slightly negative (see [36, 37]). This suggests that there is a scalar linear rising potential present, as they seem to observe the famous inversion [47, 48]. However, the European Twisted Mass Collaboration finds the P wave SOS to be negative and the D wave SOS to be small [34]. One clearly needs to go to the continuum limit before any definite conclusions can be made.

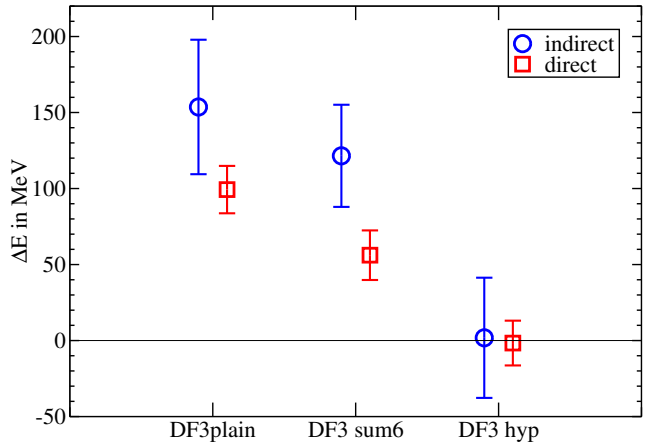

Figure 3.22: (Colour online) The Spin-Orbit splittings of P wave states for the "DF3" lattice.

In [39] Lee and Lee suggest that the absence of spin-orbit inversions can be explained by chiral radiative corrections in the potential model. Small spin-orbit splittings throughout the meson spectrum could be explained by a relativistic symmetry in the Dirac Hamiltonian discussed in [49]. This would indicate that there is a vector linear rising potential that is comparable in strength to the usual scalar linear rising potential.

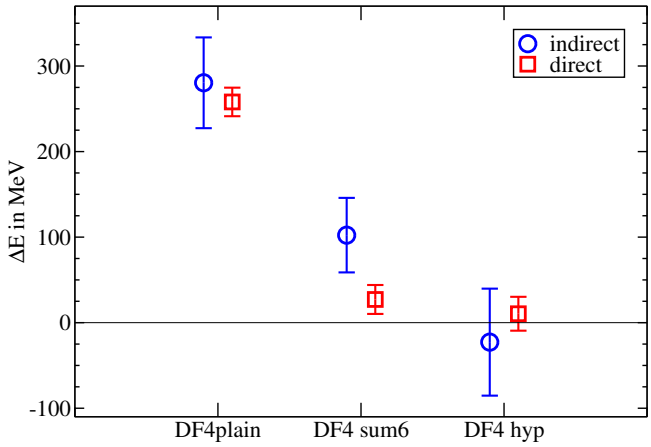

Figure 3.23: (Colour online) The Spin-Orbit splittings of P wave states for the "DF4" lattice.

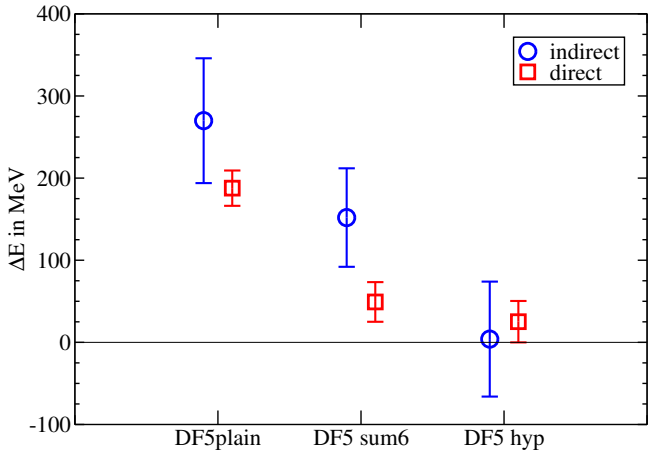

Figure 3.24: (Colour online) The Spin-Orbit splittings of P wave states for the "DF5" lattice.

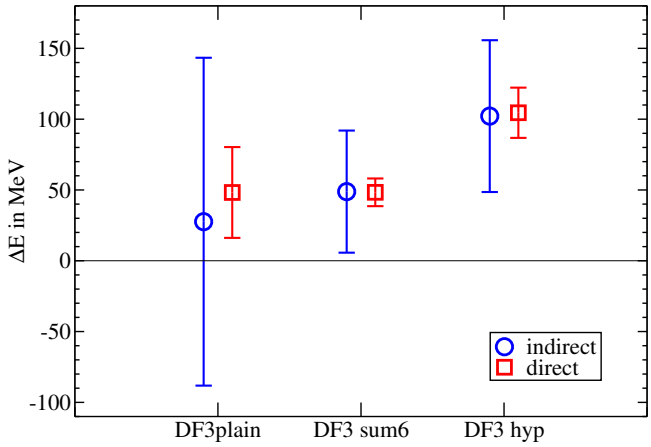

Figure 3.25: (Colour online) The Spin-Orbit splittings of D wave states for the "DF3" lattice.

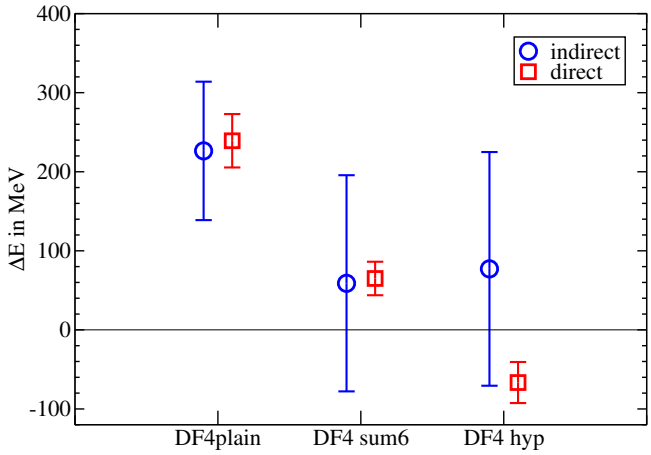

Figure 3.26: (Colour online) The Spin-Orbit splittings of D wave states for the "DF4" lattice.

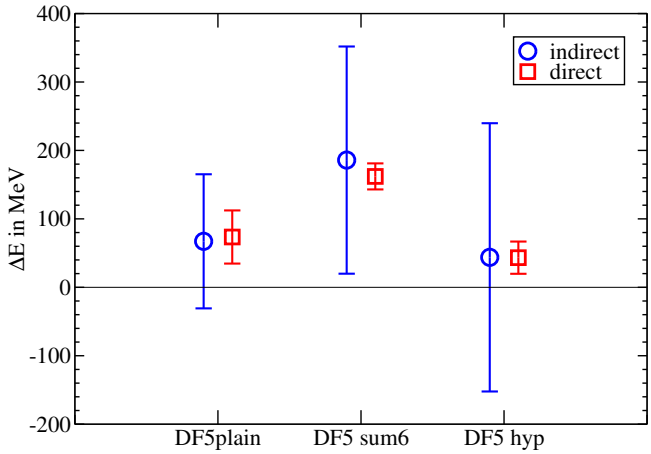

Figure 3.27: (Colour online) The Spin-Orbit splittings of D wave states for the "DF5" lattice.

Lattice	Direct	Indir.
DF3plain	0.26(4)	0.41(12)
DF3sum6	0.15(4)	0.32(9)
DF3hyp	0.00(4)	0.00(11)
DF4plain	0.69(4)	0.75(14)
DF4sum6	0.07(5)	0.27(12)
DF4hyp	0.03(5)	-0.06(17)
DF5plain	0.50(6)	0.7(2)
DF5sum6	0.13(6)	0.40(16)
DF5hyp	0.07(7)	0.0(2)

Table 3.7: P wave spin-orbit splitting $r_0\Delta E = r_0[m(1\mathrm{P}_+) - m(1\mathrm{P}_-)]$ for the different lattices. To get ΔE in GeV requires a factor 0.38(2).

Lattice	Direct	Indir.
DF3plain	0.13(9)	0.1(3)
DF3sum6	0.13(3)	0.13(11)
DF3hyp	0.28(5)	0.27(14)
DF4plain	0.64(9)	0.6(2)
DF4sum6	0.17(6)	0.2(4)
DF4hyp	-0.18(7)	0.2(4)
DF5plain	0.20(10)	0.2(3)
DF5sum6	0.43(5)	0.5(4)
DF5hyp	0.12(6)	0.1(5)

Table 3.8: D wave spin-orbit splitting $r_0\Delta E = r_0[m(1\mathrm{D}_+) - m(1\mathrm{D}_-)]$ for the different lattices. To get ΔE in GeV requires a factor 0.38(2).

Chapter 4

Radial distributions

4.1 Three-point correlation functions

In addition to the energies of the heavy-light meson states, we can also measure radial distributions on the lattice by adding a probe at distance R from the heavy quark. Two of our publications, [1] and [2], concentrate on these measurements.

We define the three-point correlation function as

$$C_3(R,T) = \langle \Gamma^\dagger U^Q \Gamma G_{q1} \Theta(R) G_{q2} \rangle. \tag{4.1}$$

We have now two light anti-quark propagators, G_{q1} and G_{q2}, and $\Theta(R)$ is the probe — see also Fig. 4.1. We have used two probes: $\boldsymbol{\gamma}_4$ for the vector (charge) and $\mathbf{1}$ for the scalar (matter) distribution. U^Q is the heavy quark propagator and Γ gives the spin structure of the state, as in the two-point correlator in Eq. (3.2).

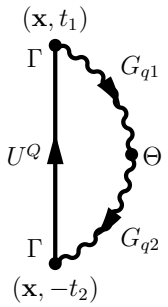

Figure 4.1: Three-point correlation function C_3.

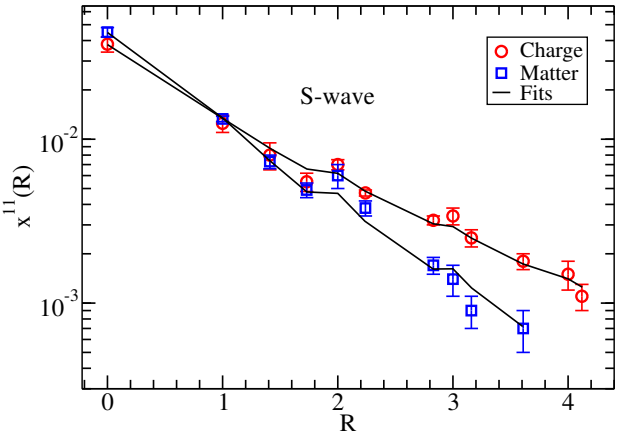

Figure 4.2: (Colour online) S wave ground state vector and scalar radial distributions $x^{11}(R)$ and discretized exponential fits using "DF2plain" configurations. Here lattice units are used ($a \approx 0.15$ fm).

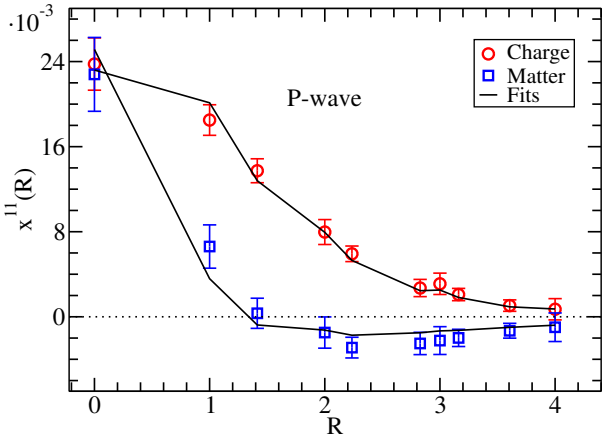

Figure 4.3: (Colour online) P$_-$ ground state vector and scalar radial distributions $x^{11}(R)$ and discretized exponential fits using "DF2plain" configurations. Here lattice units are used ($a \approx 0.15$ fm). The sign of the matter distribution is changed for clarity.

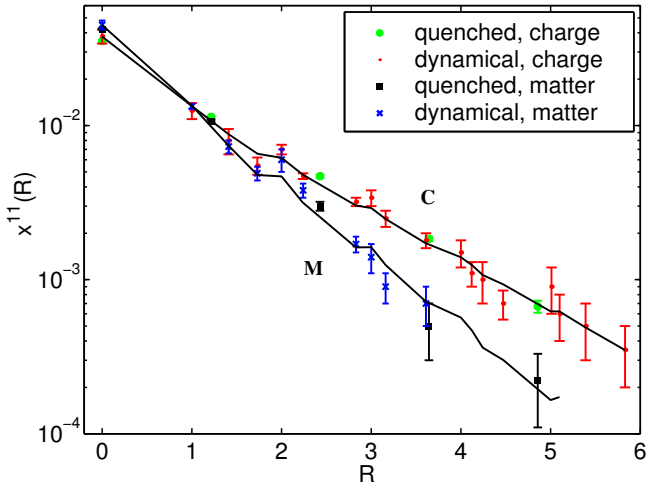

Figure 4.4: (Colour online) S wave ground state radial distributions $x^{11}(R)$. The quenched results (here scaled) are from [1] and the dynamical results are from [2]. The R is in lattice units (R/a) and $a \approx 0.15$ fm. The lines are discretized exponential fits as in Fig. 4.2.

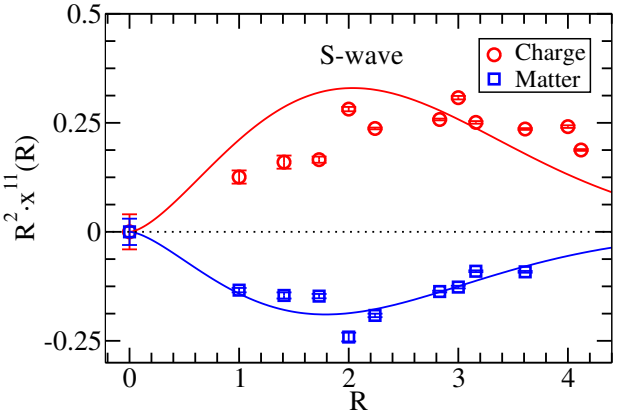

Figure 4.5: (Colour online) S wave ground state vector and scalar radial distributions $R^2x^{11}(R)$ from the "DF2plain" lattice. The solid lines are from a model (based on a one-body Dirac equation with a standard one-gluon exchange and confining potential — see Chapter 5) that is solved numerically. R is given in lattice units ($a \approx 0.15$ fm). Here the sign of the matter distribution has been changed for clarity.

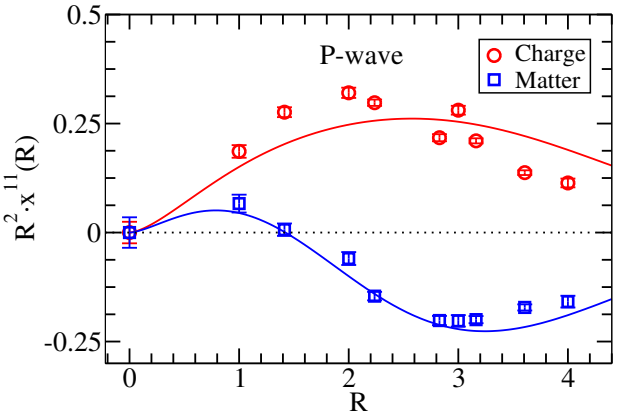

Figure 4.6: (Colour online) P$_-$ ground state vector and scalar radial distributions $R^2x^{11}(R)$ from the "DF2plain" lattice. The solid lines are from a model (based on a one-body Dirac equation with a standard one-gluon exchange and confining potential — see Chapter 5) that is solved numerically. R is given in lattice units ($a \approx 0.15$ fm). The sign of the matter distribution changed for clarity.

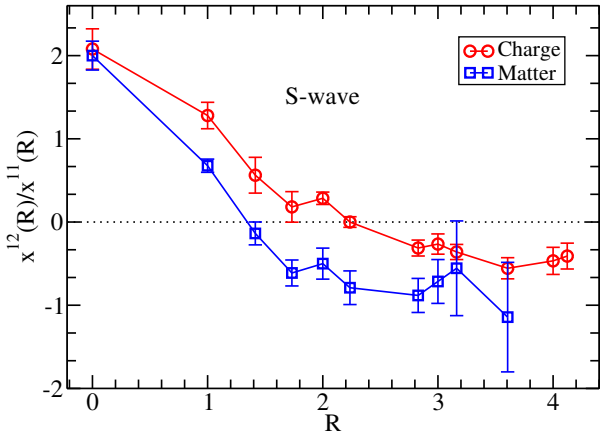

Figure 4.7: (Colour online) S wave radial distributions $x^{12}(R)/x^{11}(R)$ containing the first radially excited state using "DF2plain" configurations (Refs. [1, 2]). R is in lattice units ($a \approx 0.15$ fm).

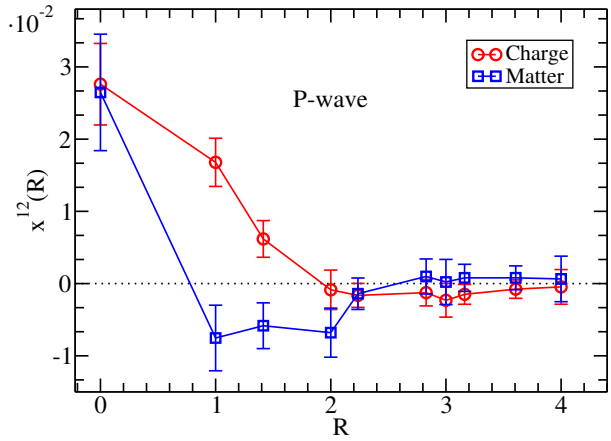

Figure 4.8: (Colour online) P$_-$ radial distributions $x^{12}(R)$ containing the first radially excited state using "DF2plain" configurations R is in lattice units ($a \approx 0.15$ fm). The sign of the matter distribution changed for clarity.

The radial distributions, $x^{ij}(R)$'s, are then extracted by fitting the C_3 with

$$C_3(R,T) \approx \sum_{i,j=1}^{N_{\max}} c_i \mathrm{e}^{-m_i t_1} x^{ij}(R) \mathrm{e}^{-m_j t_2} c_j. \tag{4.2}$$

Here $T = t_1 + t_2$ and the m_i's and c_i's are from the best fit to C_2 (Eq. (3.14)). Here x^{11} is the ground state distribution and x^{12}, for example, is the overlap between the ground state and the first excited state. The results are shown in Figs. 4.2 –4.15. These radial distributions as well as the energy differences can be treated as "experimental data" that needs understanding.

Figs. 4.2 – 4.8 compare the vector (charge) distribution with the scalar (matter) distribution. The S wave ground state matter distribution seems to drop off faster than the charge distribution (Fig. 4.2). However, at $R = 0$ the vector and scalar distributions are roughly equal, for both the S wave and the P wave ground state respectively. Note that the P wave matter distribution changes its sign (Fig. 4.3).[1] (Hence the logarithmic scale in the S wave plot but a linear scale in the P wave plot.) Now that we have the distributions, we would like to parametrize them, as the parametrized distributions would be easy to use in theoretical considerations and models. The solid lines in Figs. 4.2, 4.3 are discretized exponential fits to the "DF2plain" lattice data: we assume the radial distribution to be

[1]These general features have a natural explanation in terms of Dirac equation wave functions — see Chapter 5

of a simple form, say, an exponential $a^{\mathrm{E}} \exp[-r/r^{\mathrm{E}}]$, and see how well that fits the data. However, it is seen that the data is not smooth, but discretization (lattice) is easily seen in the distribution. Hence we prefer to use a discretized form of the exponential. It can be obtained by simply replacing in the usual Fourier transform the q^2 factors by their lattice equivalent $\frac{4}{a^2}\sum_{i=1}^{3}\sin^2(aq_i/2)$. This results in

$$\left[\mathrm{e}^{-r/r^{\mathrm{LE}}}\right]_{\mathrm{LE}} = \frac{\pi a}{2r^{\mathrm{LE}}L^3}\sum_{\mathbf{q}}\frac{\cos(\mathbf{r}\cdot\mathbf{q})}{[D+(a/r^{\mathrm{LE}})^2/4]^2}, \tag{4.3}$$

where $D = \sum_{i=1}^{3}\sin^2(aq_i/2)$. Using two exponentials in the fit, i.e.

$$C_3(\mathbf{r}) \approx \sum_{i=0,1} c_i \left[\mathrm{e}^{-r/r_i^{\mathrm{LE}}}\right]_{\mathrm{LE}} \tag{4.4}$$

we get ranges $r_0^{\mathrm{LE}}/a = 1.37(6)$, $r_1^{\mathrm{LE}}/a = 0.116(15)$ for the charge distribution and $r_0^{\mathrm{LE}}/a = 0.938(39)$, $r_1^{\mathrm{LE}}/a = 0.099(11)$ for the matter distribution (here lattice spacing $a \approx 0.15$ fm). See [2] for more details.

Seeing that we have two light quark propagators (G_{q1} and G_{q2} in Eq. 4.1) and two propagator-like terms $D + (a/r^{\mathrm{LE}})^2/4$ in Eq. 4.3, the exponential could be interpreted as a product of two non-interacting quark propagators, when viewed from the t-channel. If the momentum of the probe is divided equally between the propagators, then the appropriate momentum transfer in each propagator becomes $q/2$. If we now go to the continuum limit, the terms $D + (a/r^{\mathrm{LE}})^2/4$ give the masses of the propagating particles as $1/(2r^{\mathrm{LE}})$. In the case of the charge (vector) distribution the lowest mass would thus be about 0.48 GeV. Therefore, one interpretation would be that the constituent quark mass is about 480 MeV, leading — in a naive description where the meson consist of two non-interacting quarks — to a vector meson mass $m_{\mathrm{vector}} \approx 0.96$ GeV. Similarly the matter (scalar) distribution would predict a scalar meson of mass $m_{\mathrm{scalar}} \approx 1.4$ GeV. These vector and scalar meson masses have also been measured directly on the same lattice "DF2plain" by the UKQCD Collaboration. Their results are $am_{\mathrm{vector}} = 0.785^{+9}_{-7}$ (from [28]), which is ≈ 1.05 GeV in physical units, and $am_{\mathrm{scalar}} = 1.18(8)$ (from [50]), ≈ 1.55 GeV in physical units. The two ways of extracting the masses give consistent results. Unfortunately, it is not straightforward to identify the above particles and their masses directly with physical particles, since our light quarks are degenerate u, d quarks with a mass $m_q \approx m_s$. In addition, we do not include contributions from disconnected correlators in our lattice measurements. Fortunately the latter has been shown in Ref. [51] to be only a small effect for vector mesons. Since the light quark mass used in our calculations is approximately the strange quark mass, the closest equivalent in nature would be the $\phi(1020)$ vector meson.

	Charge			Matter		
Form (F)	LE	LY	LG	LE	LY†	LG
$c_0^{\rm F}$	0.0245(21)	0.066(3)	0.0075(7)	0.0345(26)	0.186(23)	0.0101(16)
$r_0^{\rm F}$	1.37(6)	1.78(7)	3.07(12)	0.938(39)	0.92(6)	2.14(11)
$c_1^{\rm F}$	0.373*	–0.060*	0.019(4)	0.561*	−0.207*	0.034(10)
$r_1^{\rm F}$	0.116(15)	1.12(11)	0.99(15)	0.099(11)	0.71(12)	0.70(12)
$\chi^2/n_{\rm dof}$	0.81	0.94	0.93	1.16	1.11	1.00

Table 4.1: Fits to the S wave radial distributions from the "DF2plain" lattice with discretized exponential (LE), Yukawa (LY) and Gaussian (LG) forms. Two exponentials (or Yukawa or Gaussian functions) are used in the fit. The entries marked with an asterisk are fixed in the minimization. In LY† the $R = 0$ data point is not fitted. The values are given in lattice units (i.e. r/a, with lattice spacing $a \approx 0.15$ fm).

In addition to exponentials, discretized Gaussian,

$$\left[\mathrm{e}^{-(r/r^{\rm LG})^2}\right]_{\rm LG} = \left[\frac{r^{\rm LG}\sqrt{\pi}}{aL}\right]^3 \sum_{\mathbf{q}} \cos(\mathbf{r}\cdot\mathbf{q})\, \mathrm{e}^{-(r^{\rm LG}/a)^2 D}, \tag{4.5}$$

and Yukawa,

$$\left[\frac{\mathrm{e}^{-r/r^{\rm LY}}}{r}\right]_{\rm LY} = \frac{\pi}{aL^3} \sum_{\mathbf{q}} \frac{\cos(\mathbf{r}\cdot\mathbf{q})}{D + (a/r^{\rm LY})^2/4}, \tag{4.6}$$

forms do also give good fits to the data. The values of the fit parameters are given in Table 4.1, and more details can be found in Ref. [2]. This simple approach was used only in the S wave case and tested in the P$_-$ case. The discretized exponential fit to P$_-$ charge data in Fig. 4.3 uses the values $c_0^{\rm LE} = 0.147$, $r_0^{\rm LE}/a = 0.726$, $c_1^{\rm LE} = -0.178$ and $r_1^{\rm LE}/a = 0.454$. The parameters for the corresponding matter fit are $c_0^{\rm LE} = -0.025$, $r_0^{\rm LE}/a = 1.234$, $c_1^{\rm LE} = 0.062$ and $r_1^{\rm LE}/a = 0.686$. See [2] for more details.

In Fig. 4.4 the S wave radial distributions from a quenched lattice ("Q3", here scaled) are compared with the same distributions from the "DF2plain" lattice. It is seen that in this particular case the effect of the dynamical fermions is negligible. The same "DF2plain" distributions are shown in Figs. 4.5 and 4.6, but now multiplied by R^2. This shows where the peaks are: the peak is expected to move further away from the heavy quark, as we move from the S wave ground state to higher angular momentum states. The solid lines are from our model based on one-body Dirac equation — see Chapter 5. In Figs. 4.7 and 4.8 the charge and matter first excited state distributions are compared. As expected, a node is clearly seen in these excited state distributions. The radial distributions shown in Figs. 4.2 – 4.8 are for "DF2plain".

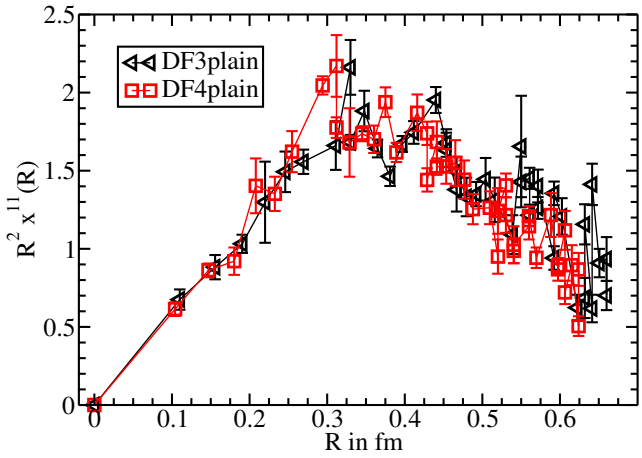

Figure 4.9: (Colour online) Radial distributions: S wave ground state $R^2x^{11}(R)$.

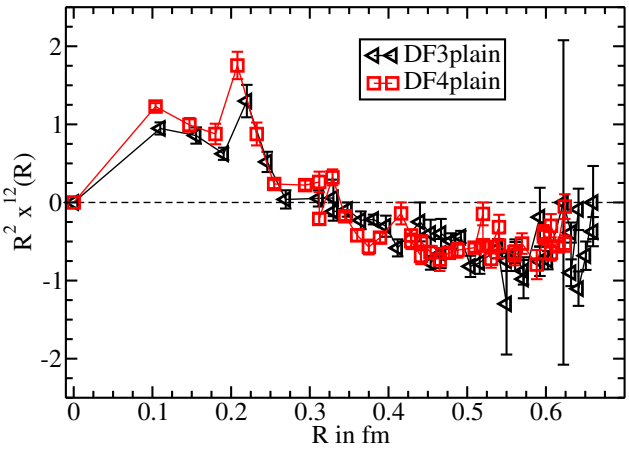

Figure 4.10: (Colour online) Radial distributions: S wave 1st excited state $R^2x^{12}(R)$.

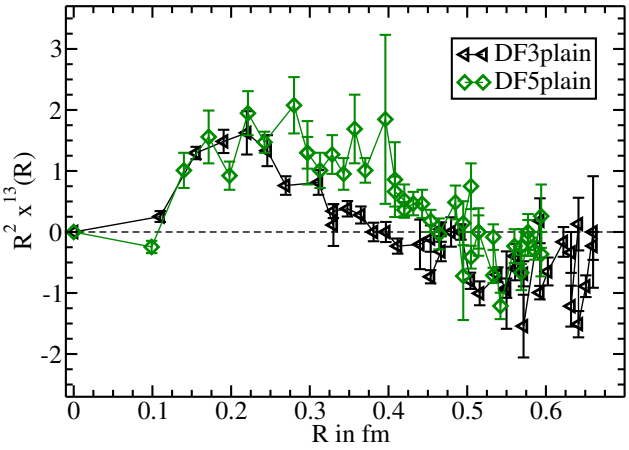

Figure 4.11: (Colour online) Radial distributions: S wave 2nd excited state $R^2x^{13}(R)$.

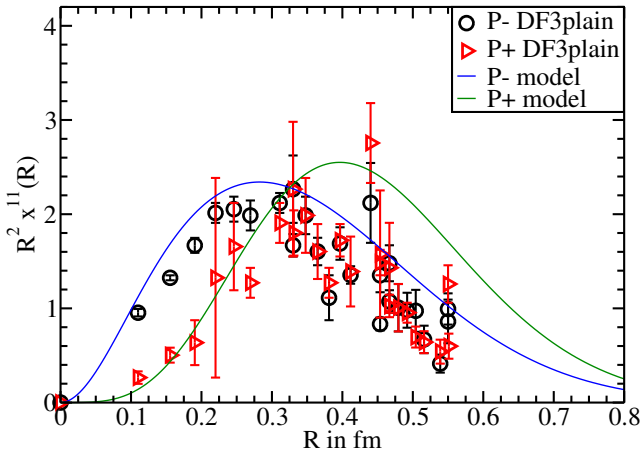

Figure 4.12: (Colour online) Radial distributions: P wave ground state $R^2x^{11}(R)$.

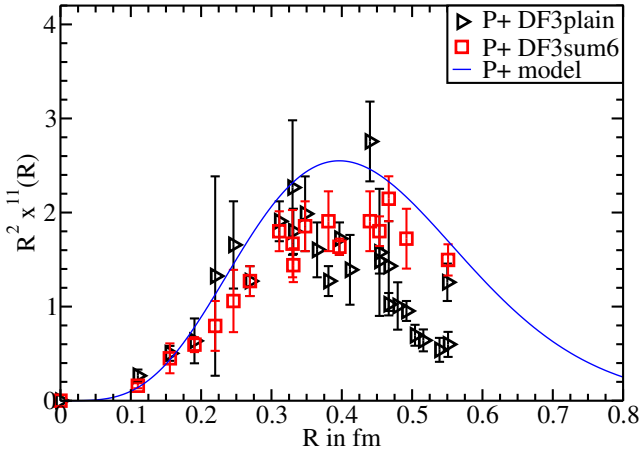

Figure 4.13: (Colour online) Radial distributions: P wave ground state $R^2x^{11}(R)$.

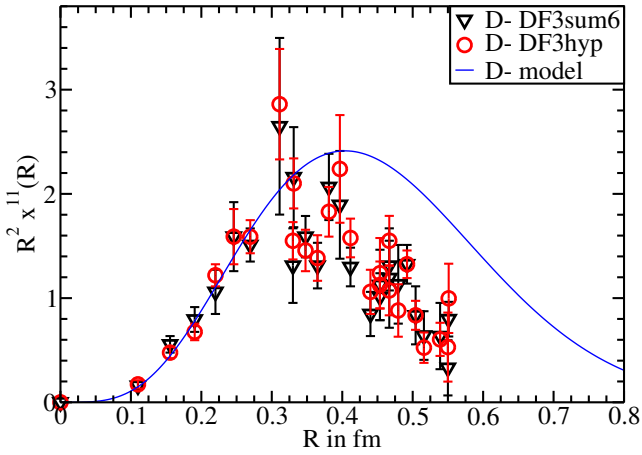

Figure 4.14: (Colour online) Radial distributions: D wave ground state $R^2x^{11}(R)$.

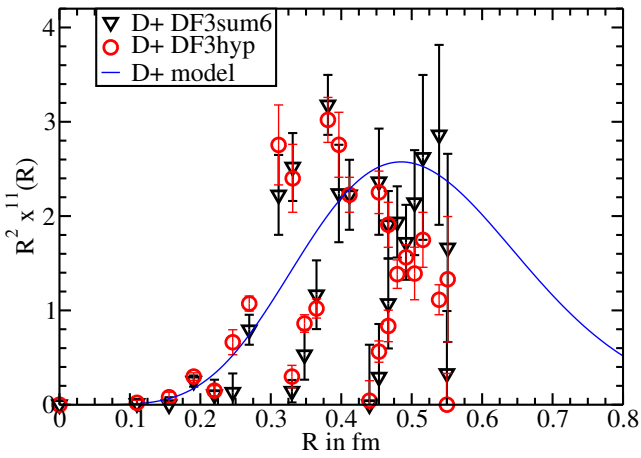

Figure 4.15: (Colour online) Radial distributions: D wave ground state $R^2x^{11}(R)$.

Results for the charge distribution from different lattices and with different smearings are compared in Figs. 4.9 – 4.15. The S wave radial distributions do not change much, as the light quark mass changes from $m_q \approx m_s$ to $m_q \approx 0.3m_s$, as can be seen in Figs. 4.9, 4.10 and 4.11. Fig. 4.9 shows the ground state, and Figs. 4.10 and 4.11 show the first and second radial excitations. Again the node of the first radial excitation is clearly seen, and in Fig. 4.11 we see a hint of two nodes, as expected for the second radial excitation. These results have been published only in conference reports [52, 53, 54].

Figs. 4.12 and 4.13 show the P wave charge distribution for our preferred lattice "DF3". In Fig. 4.12 it can be seen that the peak of the P_- distribution is closer to the heavy quark than the peak of the P_+ distribution. In Fig. 4.13 we check how much smearing in the time direction affects the distribution. For the P_+ ground state the "sum6" smearing gives smaller errors than the "plain" configurations for some R values (mostly around the peak), whereas for higher R the results with "plain" configurations can actually have slightly smaller errors than the "sum6" results. Overall the "sum6" distribution is smoother than the "plain" one.

As the D wave radial distributions are more difficult to extract than the S wave and P wave distribution, we use our smeared lattices to get as strong signal as possible. The results are shown in Figs. 4.14 and 4.15. The "sum6" and "hyp" smearings give the same results, i.e. we do not seem to benefit here from using the more elaborate "hyp" smearing. We are able to extract the distribution of the D_- state, but the D_+ signal is too weak — we get either zero or some signal with very large errors. In Figs. 4.9 – 4.15 the solid lines are predictions from the model in Chapter 5.

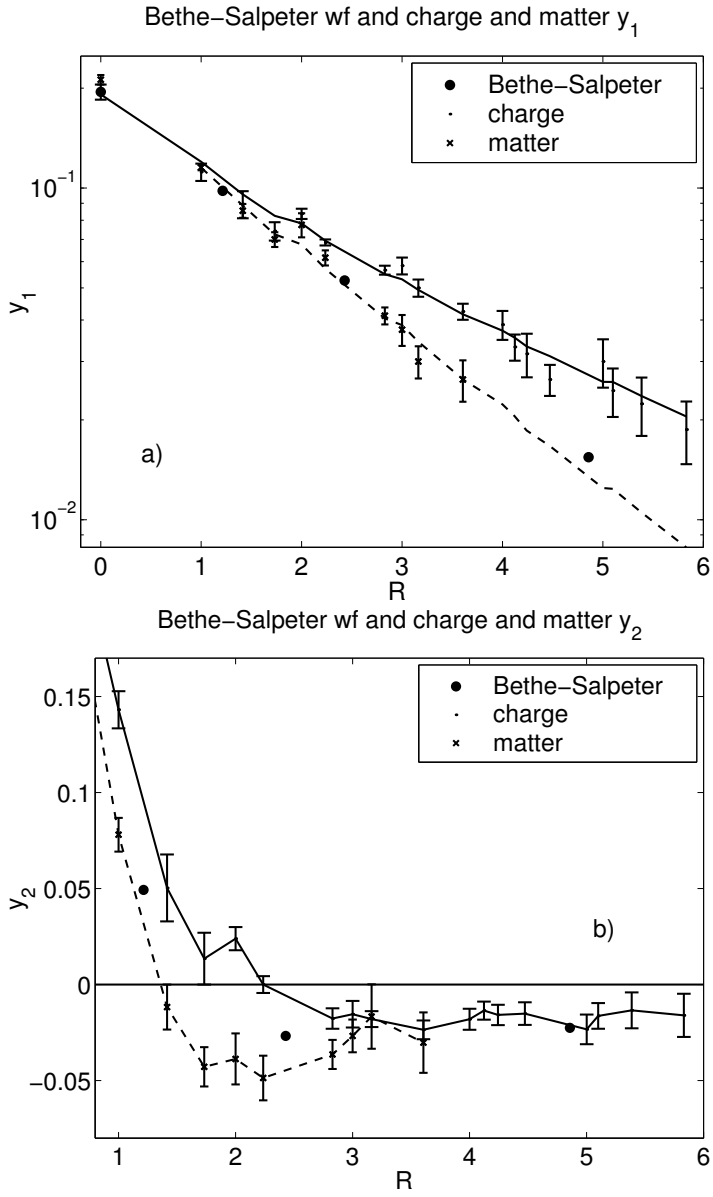

Figure 4.16: Radial distributions as wave functions: the separable form from Eq. 4.7 and comparison with Bethe-Salpeter wave functions (from [27]). R is given in lattice units ($a \approx 0.15$ fm).

In [2] also a separable fit is tried, i.e. assuming

$$x^{\alpha\beta}(R) = y_\alpha(R) y_\beta(R) \tag{4.7}$$

in Eq. (4.2). If the distributions $x^{\alpha\beta}(R)$ were to be interpreted in terms of wave functions ψ_α as $x^{\alpha\beta}(R) = \psi_\alpha \psi_\beta$, the separable form arises naturally. Then y_1 would be the ground state wave function and y_2 would be the wave function of the first radial excitation. However, such an interpretation can only have phenomenological justification. This seems to work for S wave distributions using lattices "Q3" and "DF2plain", but a reasonable fit can not be found for distributions from better lattices (e.g. "DF3") or higher excited states (P wave, D wave).

In Fig. 4.16 we compare the separable fits for "DF2plain" and Bethe-Salpeter wave functions from Ref. [27]. The Bethe-Salpeter wave functions were extracted by fitting the ground state contribution [assumed to be of the form $w_\alpha(R_1) w_\alpha(R_2) \exp(-m_\alpha T)$] to the hadronic correlator $C_{2,\alpha\alpha}(R_1, R_2, T)$. Here m_α is the mass (energy) of the state and the sink and source operators are of spatial size R_1 and R_2. The correlations are measured for a range of spatial extents R of the lattice operators used to create and destroy the meson (Eq. 3.1). The w_α from [27] have been normalized here so that the wave functions are equal at $R = 0$, i.e. $w_\alpha(0) = y_\alpha(0)$. These two types of wave function do bear some similarities, but it should be noted that there are several reasons why they should not agree in detail with each other. Firstly, the $[w_\alpha(R)]^2$ can not be identified as a charge (vector) or matter (scalar) distribution. Secondly, the Bethe-Salpeter wave functions are not independent of the operator, i.e. they depend on the path choices. Also the w_α were measured using a quenched lattice, whereas the "DF2plain" lattice that was used to measure the y_α is unquenched. More details can be found in [2].

4.2 Sum rules

In addition to measuring the three-point correlation function $C_3(R, T)$ for various values of R, the correlation where R is summed over the whole lattice is also obtained. This leads to the charge (or matter) sum rule as discussed in Ref. [1]. The actual values of this sum rule, x^{ij}_{SR}, are extracted using

$$C_3(T) \approx \sum_{i,j=1}^{N_{\max}} c_i \mathrm{e}^{-m_i t_1} x^{ij}_{\mathrm{SR}} \mathrm{e}^{-m_j t_2} c_j, \tag{4.8}$$

where the x^{ij} are now independent of R. Otherwise this is the same fit as in Eq. (4.2). The result for the charge ground state sum rule, x^{11}_{SR}, should be unity after the lattice vertex

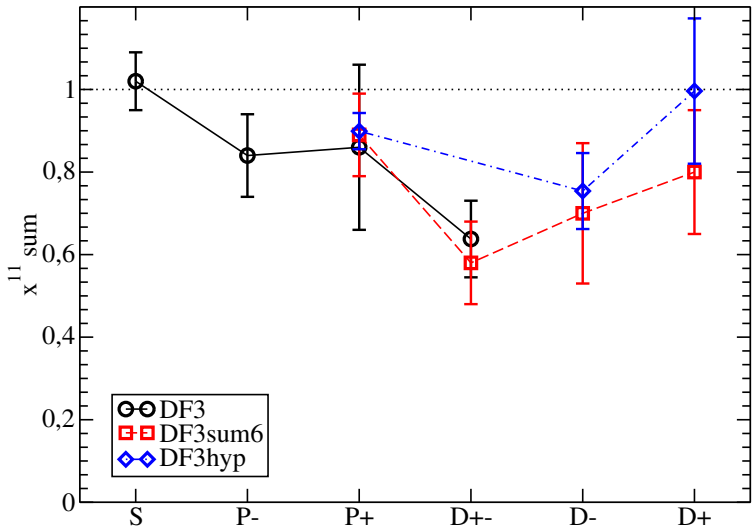

Figure 4.17: (Colour online) Sum rules for the "DF3" lattice.

correction (Z_V) is included. Here $Z_V = 0.7731(10)$ is used [55] — the value appropriate for this particular lattice. The outcome is shown in Fig. 4.17. The measured sum rule is consistent with unity only for the S wave state, the P_+ state on the "DF3plain" lattice and the D_+ on the "DF3hyp" lattice. The sum rule tends to be somewhat smaller than unity for the states with higher orbital angular momentum. Possible reasons for this could be due to the fact we are too far from the continuum limit or that the numerical signals for the contributions from large R configurations are simply too poor. However, the $x^{\alpha\beta}_{\rm SR}$ with $\alpha \neq \beta$ are, in general, much smaller than the main charge sum rules $x^{11}_{\rm SR}$ — in many cases the off-diagonal elements are consistent with zero, as expected in the continuum limit. Some examples from 3 exponential fits using the "DF3" lattice (different smearings): $x^{12}_{\rm SR} = -0.16(10)$ for the S wave state, 0.4(3) for P_-, $-0.05(9)$ for P_+, $-0.06(11)$ for D_- and $-0.03(9)$ for D_+ (lattice vertex correction included). The interpretation of $x^{22}_{\rm SR}$ is less clear (see [2, 53]).

Since we have extracted the radial distributions, we can also calculate the sum rule *indirectly*, i.e. add up explicitly all lattice measurements, say $x^{11}(x,y,z)$ (the $x^{ij}(R)$ from Eq. 4.2), with the proper weighting factors $f(x,y,z)$ up to some chosen $R = r_{\rm max}$ ($R = \sqrt{x^2+y^2+z^2}$ is the distance from the heavy quark):

$$x^{ij}_{\rm ISR} = \sum_{x,y,z}^{r_{\rm max}} x^{ij}(x,y,z) f(x,y,z). \tag{4.9}$$

This can then be compared with the *direct* sum rule estimates from Eq. 4.8. We show this comparison for the "DF3plain" S wave and P wave ground states in Figs. 4.18, 4.19 and 4.20. As we can only extract the radial distributions up to a certain R (depending on the size of the lattice and the strength of the signal), the indirect estimate falls short of the direct sum rule. For example for the "DF3plain" S wave distribution the indirect charge sum rule is 0.80(1) (up to $R = 6a \approx 0.66$ fm) compared with the direct estimate of 1.02(7). Therefore we try to estimate the contribution of the missing tail to the indirect sum rule by adding an exponential, Yukawa or Gaussian tail to the radial distribution. We match the tail to the distribution at (x,y,z)=(4,4,2) (R=6) — the largest value of R where we can measure the distribution reliably — and integrate over the tail. The total indirect sum rule becomes 0.97(4) with the exponential tail and 0.91(3) with the Gaussian tail — much closer to the direct estimate. The tail contributions can be estimated in the same way for higher excited states. Our results are given in Table 4.2. The study presented here is only exploratory.

Calculating the indirect sum rule may not seem to be very useful. However, it serves two purposes. Firstly, the observation that the direct and indirect sum rules (with tails) agree within errors is a consistency check. Secondly, the fact that — for higher partial waves — both the direct and indirect sum rules tend to be less than unity shows that contributions are being underestimated for some values of R. A comparison with the radial distributions predicted by the Dirac equation indeed suggest that for large R the P_+ and D_- lattice distributions appear to be smaller than expected from an understanding in terms of the Dirac equation (see Fig. 4.12 and Chapter 5).

The previous paragraphs have dealt with the charge sum rule, where the operator Θ in Eqs. 4.1, 4.8 is γ_4 for probing the charge distribution. We now look at the matter sum rule with $\Theta = \mathbf{1}$. The matter sum rule can be estimated by employing data from different hopping parameters κ and using the identity [56, 57]

$$x^{11}_{\text{SR, matter}} = \frac{\mathrm{d}m_1}{\mathrm{d}m_q}, \tag{4.10}$$

where m_1 is the ground state energy and m_q the valence quark mass. Using the values of m_1:s from Ref. [27] where the light quark is of about one and two strange quark masses to estimate the value of Eq. 4.10 give 0.62(14). Our results from the "DF2plain" lattice (from [2]) vary in the range 0.66–1.1 (not including the lattice vertex correction). There are indications that the vertex correction could be sizeable — from ~ 0.5 (Ref. [58]) to ~ 0.8 (Ref. [59]). The fact that $x^{11}_{\text{SR, matter}} < 1$ can be understood in terms of a potential approach using the Dirac equation (see Chapter 5).

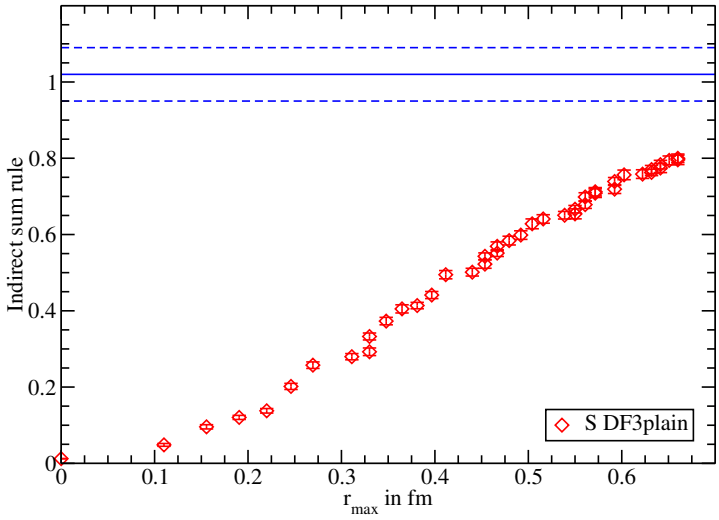

Figure 4.18: (Colour online) Indirect sum rule for the "DF3plain" S wave without the tail correction to include contributions beyond $R = 6a$. The horizontal lines show the direct sum rule and its errors.

The conclusion to this Chapter is as follows: We have extracted the radial distributions at fixed values of R, and fitted these results with discretized forms (Eqs. (4.3)–(4.6)). The parameters needed in these forms are then shown to be consistent with the corresponding vector and scalar $s\bar{s}$ mesons measured on the lattice and experiments [$\phi(1020)$]. However, an alternative R-dependent approach is to extract the radial distributions directly in the form of some simple parametrization $f(R)$ and not as above, at fixed values of R. These forms could then be compared directly with the Dirac distributions (see Chapter 5). Also these would lead to a consistent inclusion of distributions tails needed in the indirect sum rule.

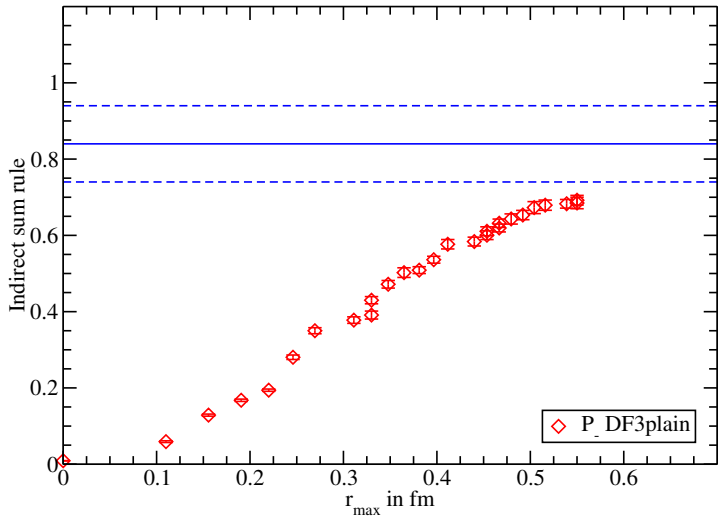

Figure 4.19: (Colour online) Indirect sum rule for the "DF3plain" P_- wave without the tail correction to include contributions beyond $R = 6a$. The horizontal lines show the direct sum rule and its errors.

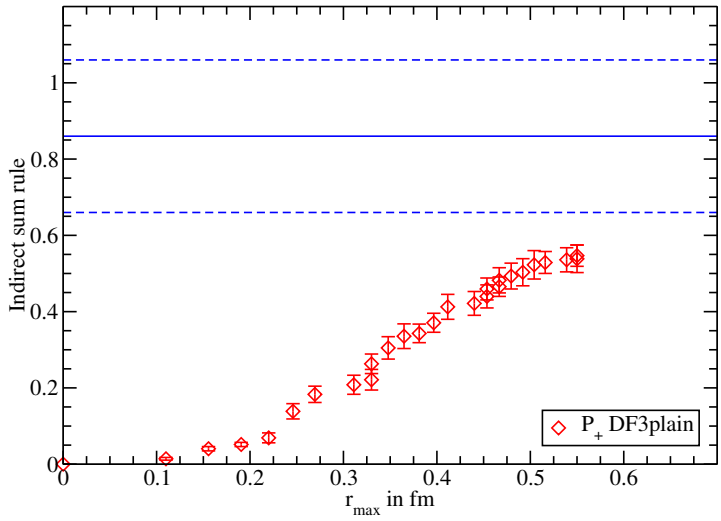

Figure 4.20: (Colour online) Indirect sum rule for the "DF3plain" P_+ wave without the tail correction to include contributions beyond $R = 6a$. The horizontal lines show the direct sum rule and its errors.

Direct sum rule	S	P_-	P_+	D_-	D_+
DF3plain	1.02(7)	0.84(10)	0.86(20)	–	–
DF3sum6	–	–	0.89(10)	0.70(17)	0.80(15)
DF3hyp	–	–	–	0.75(9)	1.00(18)
Indirect sum rule	S	P_-	P_+	D_-	D_+
no tail	0.80(1)	0.69(1)	–	–	–
with exponential tail	0.97(4)	0.94(8)	–	–	–
with Yukawa tail	–	0.88(5)	–	–	–
with Gaussian tail	0.91(3)	–	–	–	–

Table 4.2: Direct and indirect charge sum rules for the lattice "DF3". The indirect sum rules are for "DF3plain". The entries marked with a dash are not available.

Chapter 5

Modelling

5.1 A model based on the Dirac equation

Since the mass of the heavy quark is infinite, the static-light system provides an excellent testbed for modelling. For a potential description we have essentially a one-body problem. Therefore we use a simple model based on the Dirac equation to try to describe the lattice data (see [4]). The potential is not known, but we can try different potentials in the Dirac equation, solve it numerically, fit the energy differences to the lattice data and see which one of the potential choices gives the best fit. We can also use the radial distributions from the lattice as input, or we can fit only lattice energies and use the resulting wave functions as predictions that can be compared to the lattice radial distribution results.

We use the $Q\bar{Q}$ potential, which is usually taken to be of the form

$$V = -\frac{e}{R} + bR \tag{5.1}$$

(see e.g. [60]), as a starting point. We want to keep the potential fairly simple, but it has to be also flexible to be able to describe the lattice data. Therefore we choose to include a vector confining potential, $b_{\text{vec}}r$, in addition to the usual linearly rising scalar potential, $b_{\text{sc}}r$, in our model. We also have a one gluon exchange term, $a_{\text{OGE}} \cdot V_{\text{OGE}}$, where

$$V_{\text{OGE}} = -\frac{4}{3}\frac{\alpha_s(R)}{R}, \tag{5.2}$$

with the running coupling constant $\alpha_s(R)$ given by

$$\alpha_s(R) = \frac{2}{\pi}\int_0^\infty \mathrm{d}k\, \frac{\sin(kR)}{k}\alpha_s(k^2) \tag{5.3}$$

and

$$\alpha_s(k^2) = \frac{12\pi}{27}\frac{1}{\ln[(k^2+4m_g^2)/(\Lambda_{\overline{\text{QCD}}}^2)]}. \tag{5.4}$$

Here, guided by fits to various meson masses using the Blankenbecler–Sugar equation, we fix $\Lambda_{\rm QCD} = 260$ MeV and the dynamical gluon mass $m_g = 290$ MeV (see [61] for details). The potential also has a scalar term $m\omega L(L+1)$, which seems to be needed to increase the energy of D wave states. This type of term arises in flux tube models, where a flux tube's rotational energy is proportional to $L(L+1)$ (as in the Isgur–Paton flux tube model, [62]). This potential is inserted into a one-body Dirac equation, which is then solved numerically. The free parameters (e.g. the coefficients of the different terms) in the potential are fixed by doing a least squares fit to the lattice results.

The lines in the energy spectrum plot (Fig. 5.1) show three Dirac model fits from Table 5.1 with $m = 560$ MeV (the constituent quark mass, from [61]) and $a_{\rm OGE} = 1.00$. We have to fix $a_{\rm OGE}$, as attempts to vary it (along with other parameters) easily lead to instabilities. The solid line, labelled "fit 1", is a fit to three "DF3hyp" energy differences: $1P_-$ and $1D_-$ with respect to the ground state, and the P wave spin-orbit splitting (direct estimate) SOS(1P) [i.e. $E(1P_+) - E(1P_-)$]. The fit to these energies is acceptable with total $\chi^2 = 1.83$. However, as soon as a fourth state [e.g. SOS(D)] is added a good χ^2 can no longer be achieved. The dashed line, "fit 2", shows an attempt to fit "DF3hyp" $1P_-$, SOS(1P), $1D_-$ and SOS(1D). The χ^2 is very poor, and letting $a_{\rm OGE}$ vary does not help, only leading to unphysical values for the parameters. Using a different constituent quark mass, say $m = 490$ MeV from [47, 48], gives basically the same fits (the changes are minimal). "Fit 3" is a fit to "DF3sum6" $1P_-$, SOS(1P), $1D_-$ and SOS(1D), and gives a much better χ^2 ($\chi^2 = 2.1$) than "fit 2". It is shown in the figure for comparison. The fits to "DF3sum6" energies are also shown in Table 5.1. In Fig. 5.2 the same Dirac model fits are shown as predictions for the excited states. Here it can be seen that the fit is about 500 MeV lower than the lattice results, and the shift seems to be constant for both lattices ("DF3sum6" and "DF3hyp") for all states, except the 2S. There is no obvious reason why the Dirac model should underestimate the first radial excitations by a constant amount, but a term of the form $0.5(n-1)$ GeV could be included in the model to improve the fit to excited states and be interpreted as a flux tube effect in the same philosophy as the ωL(L + 1) term. However, as the fit to the ground state energies is not good, this improvement is not pursued.

The earlier fits to "DF2plain" data shown in Figs. 4.5 and 4.6 are with a simple potential

$$V_{\rm vector} = -\frac{e}{R}, \quad V_{\rm scalar} = bR. \tag{5.5}$$

Here $e = 0.6 \cdot \hbar c$, $b = 1.27$ MeV/fm and $m = 100$ MeV. The fits shown in Figs. 4.12 – 4.15 are also not the most recent ones: the fits do use the more sophisticated potential described earlier in this Chapter, but the fit parameters $m = 88$ MeV, $a_{\rm OGE} = 0.81$,

$b_{\rm sc} = 1.14$ GeV/fm, $b_{\rm vec} = 1.12$ GeV/fm and $\omega = 0.028$ have not been optimized to the latest data. Even though these Dirac model fits are not perfect fits to the lattice energies quantitatively, they have several good features. In particular the Dirac model wave functions show qualitative agreement with the lattice distributions, and can reproduce their general key features as follows. If the light quark is treated as a particle in a potential generated by the heavy quark, as here, then its wave function will be of the form (F, G), where F is the upper (usually large) and G is the lower (usually small) component of the Dirac wave function. The charge density can then be expressed as

$$x_C^{11}(R) = F^2(R) + G^2(R) \tag{5.6}$$

and the matter density as

$$x_M^{11}(R) = F^2(R) - G^2(R). \tag{5.7}$$

This gives a natural explanation to the fact that the matter distribution drops off faster than the charge distribution (Fig. 4.2), as $|F(R)| \gg |G(R)|$ for small R, whereas $|F(R)| \sim |G(R)|$ for large R (see Fig. 5.3). Note that the $|G(R)|$ being much smaller than $|F(R)|$ for small R also means that $x_C^{11} \approx x_M^{11}$ at $R = 0$, which is also seen in the lattice data. Also the node in the P_- matter distribution in Fig. 4.3 is easy to understand in terms of the Dirac wave functions, as the expression in Eq. 5.7 has a minus sign. For the P_- state G is larger than F for small R, but as R increases G goes to zero and $F(R) > G(R)$ (see Fig. 5.4). No node is seen in the P_- lattice charge distribution, as expected. In Fig. 5.5 the wave functions F and G for the P_+ state are shown for comparison. These Dirac wave function plots are predictions from "fit 3" in Table 5.1, and are meant as examples.

The sum rules can also be expressed in terms of the Dirac wave functions The charge of the $\bar{q}$ is simply

$$I_C = 4\pi \int \mathrm{d}R R^2 \big[F^2(R) + G^2(R)\big], \tag{5.8}$$

which by the normalisation used here will be unity. However, when the charge operator (γ_4) is replaced by the matter operator (unity), then the corresponding integral is

$$I_M = 4\pi \int \mathrm{d}R R^2 \big[F^2(R) - G^2(R)\big]. \tag{5.9}$$

In the non-relativistic limit $I_C = I_M$, but as relativistic effects enter (i.e. G^2 increases from zero), then I_M becomes less than I_C, i.e. less than unity. This is clearly seen in Section 4.2.

Case	$b_{\rm sc}$	$b_{\rm vec}$	ω	total χ^2	Fit
DF3sum6					
P_, SOS(1P)	1.168(2)	0.0	0.0	7.8	
P_, SOS(1P)	0.86(13)	0.57(18)	0.0	0.0	
P_, SOS(1P), D_	0.372(14)	0.0	0.0916(14)	4.5	
P_, SOS(1P), D_, SOS(1D)	0.265(4)	0.571(13)	0.0696(11)	2.1	3
DF3hyp					
P_, SOS(1P)	1.294(10)	0.0	0.0	0.54	
P_, SOS(1P)	1.40(18)	-0.2(2)	0.0	0.00	
P_, SOS(1P), D_	0.763(9)	0.0	0.0554(9)	1.83	1
P_, SOS(1P), D_, SOS(1D)	0.48(5)	0.26(2)	0.066(5)	34.3	2

Table 5.1: Dirac model fits for "DF3". Here $a_{\rm OGE} = 1.0$ and constituent quark mass $m = 560$ MeV. The $b_{\rm sc}$ and $b_{\rm vec}$ are given in GeV/fm. Fits are attempted for "DF3sum6" and "DF3hyp". A "perfect" fit (2 fit parameters, 2 data points) can be found for P_ and the P wave spin-orbit splitting, if both scalar and vector linear potentials are used. However, all P and D wave data [P_, SOS(1P), D_, SOS(1D)] can not be fitted using the two linear rising potentials and adding a scalar term $m\omega L(L+1)$ still does not give a good χ^2.

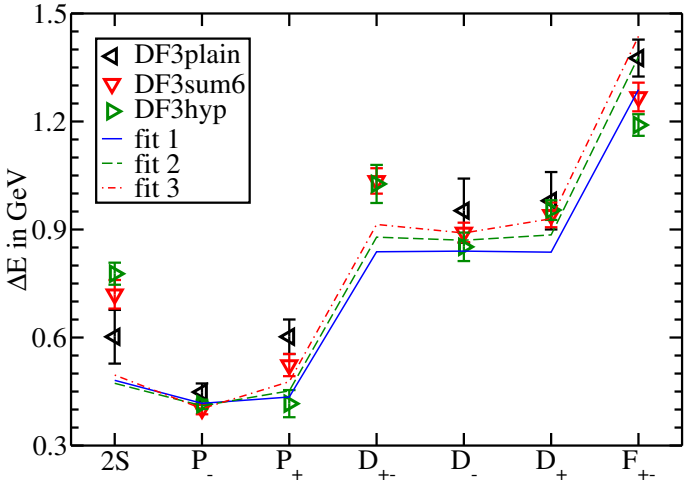

Figure 5.1: (Colour online) Energy spectrum of the heavy-light meson and three Dirac model fits. "Fit 1" is a fit to "DF3hyp" 1P_, SOS(1P) and 1D_, whereas "fit 2" is an attempt to fit "DF3hyp" 1P_, SOS(1P), 1D_ and SOS(1D). "Fit 3" is a fit to "DF3sum6" 1P_, SOS(1P), 1D_ and SOS(1D) (see Table 5.1), and is shown here for comparison.

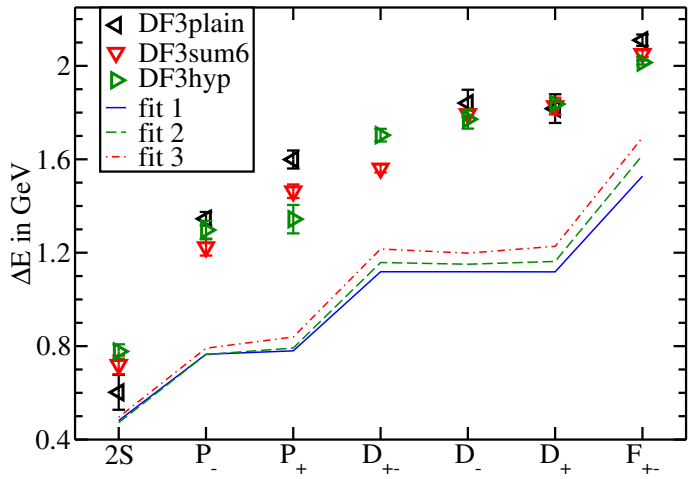

Figure 5.2: (Colour online) Energies of the first radial excitations of the heavy-light meson and the same Dirac model fits shown in Fig. 5.1.

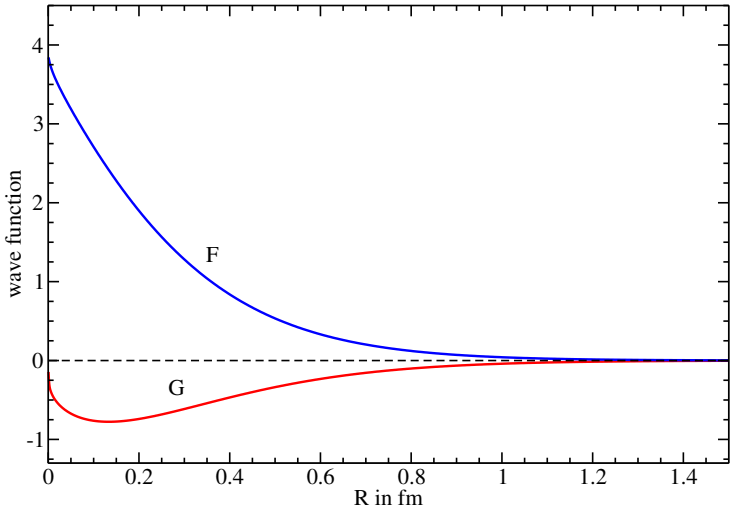

Figure 5.3: (Colour online) Dirac wave functions F and G for the S wave ground state from "fit 3" in Table 5.1. This is just an example what the Dirac wave functions look like.

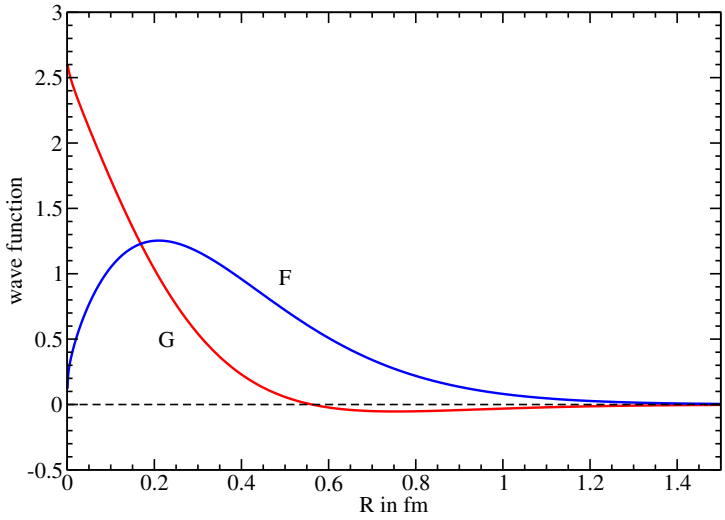

Figure 5.4: (Colour online) Dirac wave functions F and G for the P_- ground state from "fit 3" in Table 5.1. This is just an example what the Dirac wave functions look like.

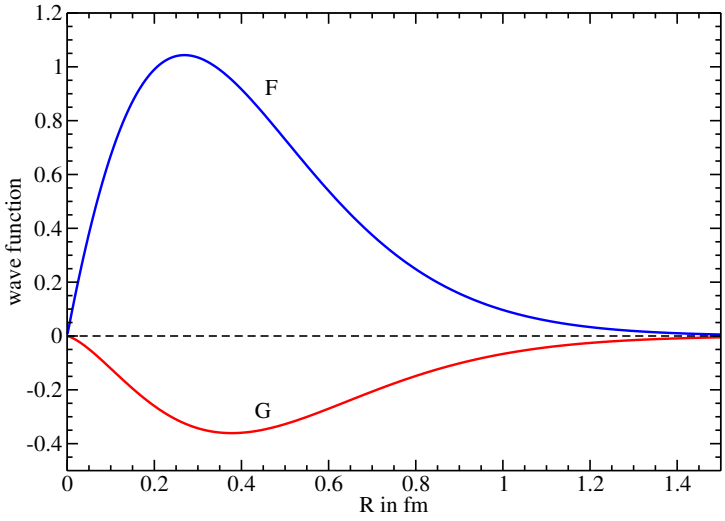

Figure 5.5: (Colour online) Dirac wave functions F and G for the P_+ ground state from "fit 3" in Table 5.1. This is just an example what the Dirac wave functions look like.

Chapter 6

Conclusions and outlook

In this thesis we have presented a study of the heavy-light meson energy spectrum and radial distributions of the ground state and several excited states. The calculations were done using lattice QCD, as computer simulations are the best tool available for such low energy QCD systems.

The key results are the energies of the P wave states, the spin-orbit splittings and the new radial distribution data. Firstly, we predict that the two lowest B_s meson P wave states with $J^P = 0^+$ and 1^+ are very near the BK threshold, indicating that these resonances should be narrow. They have not been observed experimentally yet. The extracted energies of the two higher P wave states, $J^P = 1^+$ and 2^+, are in agreement with the experimental results, which demonstrates again that lattice QCD succeeds as an effective tool in QCD studies. We are also able to extract the energies of several other excited states, including D wave states and their radial excitations.

Secondly, we have paid a lot of attention to extract the P wave and D wave spin-orbit splittings, i.e. $m(\mathrm{P}_+) - m(\mathrm{P}_-)$ and $m(\mathrm{D}_+) - m(\mathrm{D}_-)$. We get the P wave SOS to be consistent with zero, whereas some other lattice groups get clearly positive or negative results (see discussion in Section 3.6). Also the D wave SOS results differ: we get a positive SOS, but for example the TrinLat group sees the famous inversion (i.e. SOS is negative — namely the L_- state being higher in energy than the L_+ state). The spin-orbit splittings can tell us a lot about the interaction between the quarks, as they are rather sensitive to the confining potential. For example, the inversion is expected for higher angular momentum states, if the potential has a scalar linearly rising potential in addition to the $1/r$-type one-gluon exchange term. On the other hand, if a linearly rising vector confining potential is added, and if these two confining potentials (vector and scalar) are similar in strength, then the spin-orbit splittings are expected to be very small

throughout the energy spectrum. For example, the perturbative approach in Ref. [47] would predict the spin-orbit term to be

$$H_{\mathrm{SO}} \xrightarrow[m_Q \gg m_q]{} \frac{1}{2m_q^2}\Big\{\frac{4}{3}\frac{\alpha_s}{r^3} - (b-c)\frac{1}{r}\Big\} \times \big[\bar{\mathrm{L}} \cdot \bar{\mathrm{S}}_q\big], \tag{6.1}$$

when one of the quarks is much heavier than the other. Here b, c are the strengths of the scalar and vector confining potentials respectively. We see that if $c \approx b$, the contributions from the two linear rising potentials cancel leaving only the one-gluon exchange contribution. However, more precise lattice calculations are needed before any definitive conclusions can be made.

Thirdly, we have extracted the radial distributions of the S wave state (ground state and radial excitations) and some orbitally excited states (P wave and D wave). So there is now an abundance of data that can be used for example in model building. A model based on a one-body Dirac equation with one-gluon exchange and confining potentials can reproduce the main features of the distributions at a qualitative level. More precise calculations are needed, as well as a better parametrization of the data. A more refined potential description can hopefully help in understanding the underlying interaction better. However, it should be noted that the one-body Dirac equation model presented in this thesis (with the potentials that were used here) is not good enough to describe the entire lattice energy spectrum at a quantitative level. Therefore, one should be very careful in using such simple potentials to describe the interaction between quarks in general. Perhaps, a less ambitious view is to consider the Dirac equation approach as simply a condensed way of parametrizing the abundance of heavy-light meson data without expecting a deeper understanding of the potentials needed.

We are still far away from the ultimate goal of understanding multi-quark systems and potentials. The study of heavy-light mesons provides a good stepping stone, but the calculations should be extended to three-quark and four-quark systems. A natural continuation to this heavy-light meson study would be, for example, measuring the energy spectrum and the radial distribution of the light quark in a QQq baryon (a baryon consisting of two heavy quarks and one light quark) on a lattice. To our knowledge these lattice measurements have not been done before, and the results could be used in modelling baryon decay and scattering experiments. The closest equivalent in nature would be the doubly-charmed $\Xi(cc)$ baryon (seen in some experiments at 3518.9 ± 0.9 MeV — see [5]), unless a bbu, bbd or a bbs baryon is discovered in some future experiment.

Bibliography

[1] **UKQCD** Collaboration, A. M. Green, J. Koponen, P. Pennanen, and C. Michael, "The charge and matter radial distributions of heavy-light mesons calculated on a lattice," *Phys. Rev. D* **65** (2002) 014512, `hep-lat/0105027`.

[2] **UKQCD** Collaboration, A. M. Green, J. Koponen, P. Pennanen, and C. Michael, "The charge and matter radial distributions of heavy-light mesons calculated on a lattice with dynamical fermions," *Eur. Phys. J.* **C28** (2003) 79–95, `hep-lat/0206015`.

[3] **UKQCD** Collaboration, A. M. Green, J. Koponen, C. McNeile, C. Michael, and G. Thompson, "Excited B mesons from the lattice," *Phys. Rev.* **D69** (2004) 094505, `hep-lat/0312007`.

[4] **UKQCD** Collaboration, J. Koponen, "Energies of B_s meson excited states - a lattice study," *Phys. Rev.* **D78** (2008) 074509, `0708.2807 (hep-lat)`.

[5] **Particle Data Group** Collaboration, C. Amsler *et. al.*, "Review of particle physics," *Phys. Lett.* **B667** (2008) 1.

[6] J. L. Rosner, "Theoretical issues in b physics," *Eur. Phys. J.* **C34** (2004) S365–S374.

[7] **BABAR** Collaboration, B. Aubert *et. al.*, "Observation of a narrow meson decaying to $D_s^+\pi^0$ at a mass of 2.32 GeV/c^2," *Phys. Rev. Lett.* **90** (2003) 242001, `hep-ex/0304021`.

[8] **CLEO** Collaboration, D. Besson *et. al.*, "Observation of a narrow resonance of mass 2.46 GeV/c^2 in the $D_s^{*+}\pi^0$ final state, and confirmation of the $D_{sJ}^*(2317)$," *AIP Conf. Proc.* **698** (2004) 497–502, `hep-ex/0305017`.

[9] **Belle** Collaboration, K. Abe *et. al.*, "Study of $B^- \to D^{**0}\pi^-(D^{**0} \to D^{(*)+}\pi^-)$ decays," *Phys. Rev.* **D69** (2004) 112002, `hep-ex/0307021`.

[10] R. K. Mommsen, "B_c and excited B states: A Tevatron review," *Nucl. Phys. Proc. Suppl.* **170** (2007) 172–176, hep-ex/0612003.

[11] **CDF** Collaboration, T. Aaltonen *et. al.*, "Observation of orbitally excited B_s mesons," *Phys. Rev. Lett.* **100** (2008) 082001, 0710.4199 (hep-ex).

[12] **D0** Collaboration, V. M. Abazov *et. al.*, "Observation and properties of the orbitally excited B^*_{s2} meson," *Phys. Rev. Lett.* **100** (2008) 082002, 0711.0319 (hep-ex).

[13] A. M. Green, J. Lukkarinen, P. Pennanen, and C. Michael, "A study of degenerate four quark states in SU(2) lattice Monte Carlo," *Phys. Rev.* **D53** (1996) 261–272, hep-lat/9508002.

[14] A. M. Green and P. Pennanen, "A model for multi-quark systems," *Phys. Lett.* **B426** (1998) 243–250, hep-lat/9709124.

[15] A. M. Green and P. Pennanen, "An interquark potential model for multi-quark systems," *Phys. Rev.* **C57** (1998) 3384–3391, hep-lat/9804003.

[16] P. Pennanen, A. M. Green, and C. Michael, "Four-quark flux distribution and binding in lattice SU(2)," *Phys. Rev.* **D59** (1999) 014504, hep-lat/9804004.

[17] A. M. Green, J. Koponen, and P. Pennanen, "A variational fit to the lattice energy of two heavy-light mesons," *Phys. Rev. D* **61** (2000) 014014, hep-ph/9902249.

[18] H. J. Rothe, *Lattice gauge theories: An Introduction*, vol. 59 of *World Scientific Lecture Notes in Physics*. World Scientific, 1997.

[19] B. Sheikholeslami and R. Wohlert, "Improved continuum limit lattice action for QCD with Wilson fermions," *Nucl. Phys.* **B259** (1985) 572.

[20] K. G. Wilson, "Confinement of quarks," *Phys. Rev. D* **10** (Oct, 1974) 2445–2459.

[21] C. McNeile, "Meson and baryon spectroscopy on a lattice," in *Hadronic Physics from Lattice QCD* (A. M. Green, ed.), vol. 9 of *International Review of Nuclear Physics*, ch. 1, pp. 1–101. World Scientific, 2004.

[22] M. Lüscher, S. Sint, R. Sommer, P. Weisz, and U. Wolff, "Non-perturbative O(a) improvement of lattice QCD," *Nucl. Phys.* **B491** (1997) 323–343, hep-lat/9609035.

[23] R. G. Edwards, U. M. Heller, and T. R. Klassen, "The Schrödinger functional and non-perturbative improvement," *Nucl. Phys. Proc. Suppl.* **63** (1998) 847–852, `hep-lat/9710054`.

[24] **ALPHA** Collaboration, K. Jansen and R. Sommer, "O(a) improvement of lattice QCD with two flavors of Wilson quarks," *Nucl. Phys.* **B530** (1998) 185–203, `hep-lat/9803017`.

[25] I. Montvay and G. Munster, *Quantum fields on a lattice*. Cambridge University Press, 1994.

[26] A. M. Green, ed., *Hadronic Physics from Lattice QCD*, vol. 9 of *International Review of Nuclear Physics*. World Scientific, 2004.

[27] **UKQCD** Collaboration, C. Michael and J. Peisa, "Maximal variance reduction for stochastic propagators with applications to the static quark spectrum,," *Phys. Rev.* **D58** (1998) 034506.

[28] **UKQCD** Collaboration, C. R. Allton, S. P. Booth, K. C. Bowler, M. Foster, J. Garden, A. C. Irving, R. D. Kenway, C. Michael, J. Peisa, S. M. Pickles, J. C. Sexton, Z. Sroczynski, M. Talevi, and H. Wittig, "Light hadron spectroscopy with O(a) improved dynamical fermions," *Phys. Rev.* **D60** (1999) 034507.

[29] **UKQCD** Collaboration, C. R. Allton, S. P. Booth, K. C. Bowler, J. Garden, A. Hart, D. Hepburn, A. C. Irving, B. Joó, R. D. Kenway, C. M. Maynard, C. McNeile, C. Michael, S. M. Pickles, J. C. Sexton, K. J. Sharkey, Z. Sroczynski, M. Talevi, M. Teper, and H. Wittig, "Effects of nonperturbatively improved dynamical fermions in QCD at fixed lattice spacing," *Phys. Rev.* **D65** (2002) 054502.

[30] **UKQCD** Collaboration, C. R. Allton, A. Hart, D. Hepburn, A. C. Irving, B. Joó, C. McNeile, C. Michael, and S. V. Wright, "Improved Wilson QCD simulations with light quark masses," *Phys. Rev.* **D70** (2004) 014501.

[31] **UKQCD** Collaboration, P. Lacock, C. Michael, P. Boyle, and P. Rowland, "Orbitally excited and hybrid mesons from the lattice," *Phys. Rev.* **D54** (1996) 6997.

[32] A. Hasenfratz and F. Knechtli, "Flavor symmetry and the static potential with hypercubic blocking," *Phys. Rev.* **D64** (2001) 034504.

[33] M. Della Morte, A. Shindler, and R. Sommer, "On lattice actions for static quarks," *JHEP* **0508** (2005) 051.

[34] **ETM** Collaboration, . K. Jansen, C. Michael, A. Shindler, and M. Wagner, "The static-light meson spectrum from twisted mass lattice QCD," `0810.1843 (hep-lat)`.

[35] T. Burch, C. Hagen, C. B. Lang, M. Limmer, and A. Schafer, "Excitations of singly beautiful hadrons," `0809.1103 (hep-lat)`.

[36] J. Foley, A. O. Cais, M. Peardon, and S. M. Ryan, "Orbital and radial excitations of static-light mesons," *PoS* **LAT2006** (2006) 196.

[37] J. Foley, A. O'Cais, M. Peardon, and S. M. Ryan, "Radial and orbital excitations of static-light mesons," *Phys. Rev.* **D75** (2007) 094503, `hep-lat/0702010`.

[38] V. Poireau, "New resonances and meson spectroscopy at BaBar and Belle," `0705.3716 (hep-ex)`.

[39] I. W. Lee and T. Lee, "Why there is no spin-orbit inversion in heavy-light mesons," *Physical Review D (Particles and Fields)* **76** (2007), no. 1 014017.

[40] G. S. Bali, "The $D_{sJ}^{+}(2317)$: What can the lattice say?," *Phys. Rev.* **D68** (2003) 071501, `hep-ph/0305209`.

[41] R. Lewis and R. M. Woloshyn, "S and P-wave heavy-light mesons in lattice NRQCD," *Phys. Rev.* **D62** (2000) 114507, `hep-lat/0003011`.

[42] **UKQCD** Collaboration, A. Dougall, R. D. Kenway, C. M. Maynard, and C. McNeile, "The spectrum of D_s mesons from lattice QCD," *Phys. Lett.* **B569** (2003) 41–44, `hep-lat/0307001`.

[43] **UKQCD** Collaboration, P. Boyle, "Comprehensive spectroscopy of D, D_s and charmonium systems from relativistic lattice QCD," *Nucl. Phys. Proc. Suppl.* **53** (1997) 398–400.

[44] J. Hein *et. al.*, "Scaling of the B and D meson spectrum in lattice QCD," *Phys. Rev.* **D62** (2000) 074503, `hep-ph/0003130`.

[45] S. Collins *et. al.*, "Sea quark effects in B spectroscopy and decay constants," *Phys. Rev.* **D60** (1999) 074504, `hep-lat/9901001`.

[46] P. Colangelo, F. De Fazio, and S. Nicotri, "$D_{sJ}(2860)$ resonance and the $s_\ell^P = \frac{5}{2}^-$ $c\bar{s}$ ($c\bar{q}$) doublet," *Phys. Lett.* **B642** (2006) 48–52, hep-ph/0607245.

[47] H. J. Schnitzer, "Spin structure in meson spectroscopy with an effective scalar confinement of quarks," *Phys. Rev.* **D18** (1978) 3482.

[48] H. J. Schnitzer, "Where are the inverted multiplets of meson spectroscopy?," *Phys. Lett.* **B226** (1989) 171.

[49] P. R. Page, J. T. Goldman, and J. N. Ginocchio, "Relativistic symmetry suppresses quark spin-orbit splitting," *Phys. Rev. Lett.* **86** (2001) 204–207, hep-ph/0002094.

[50] **UKQCD** Collaboration, C. McNeile and C. Michael, "Mixing of scalar glueballs and flavour-singlet scalar mesons," *Phys. Rev.* **D63** (2001) 114503, hep-lat/0010019.

[51] C. McNeile, C. Michael, and K. J. Sharkey, "Flavor singlet mesons in qcd," *Phys. Rev. D* **65** (Dec, 2001) 014508.

[52] **UKQCD** Collaboration, A. M. Green, J. Ignatius, M. Jahma, J. Koponen, C. McNeile, and C. Michael, "B_s meson excited states from the lattice," *PoS* **LAT2005** (2005) 205, hep-lat/0509161.

[53] **UKQCD** Collaboration, J. Koponen, "Energies and radial distributions of B_s mesons: The effect of hypercubic blocking," *PoS* **LAT2006** (2006) 112, hep-lat/0703011.

[54] J. Koponen, "Energies and radial distributions of B_s mesons on the lattice," *Acta Phys. Polon.* **B38** (2007) 2893–2900, hep-lat/0702006.

[55] **QCDSF–UKQCD** Collaboration, T. Bakeyev, M. Gockeler, R. Horsley, D. Pleiter, P. E. L. Rakow, G. Schierholz, and H. Stuben, "Non-perturbative renormalisation and improvement of the local vector current for quenched and unquenched Wilson fermions," *Phys. Lett.* **B580** (2004) hep-lat/0305014.

[56] M. S. Foster, *Adjoint sources, disconnected loops and other fruit of lattice QCD.* PhD thesis, University of Liverpool, 1998.

[57] M. Foster and C. Michael, "Quark mass dependence of hadron masses from lattice QCD," *Phys. Rev. D* **59** (Feb, 1999) 074503.

[58] M. Göckeler, R. Horsley, A. C. Irving, D. Pleiter, P. E. L. Rakow, G. Schierholz, H. Stüben, and J. M. Zanotti, "Estimating the unquenched strange quark mass from the lattice axial Ward identity," *Phys. Rev.* **D73** (2006) 054508, hep-lat/0601004.

[59] L. Giusti and A. Vladikas, "RI/MOM renormalization window and Goldstone pole contamination," *Phys. Lett.* **B488** (2000) 303–312, hep-lat/0005026.

[60] G. S. Bali, "QCD forces and heavy quark bound states," *Phys. Rept.* **343** (2001) 1–136, hep-ph/0001312.

[61] T. A. Lähde, C. J. Nyfält, and D. O. Riska, "Spectra and M1 decay widths of heavy-light mesons," *Nucl. Phys.* **A674** (2000) 141–167, hep-ph/9908485.

[62] N. Isgur and J. E. Paton, "A flux tube model for hadrons in QCD," *Phys. Rev.* **D31** (1985) 2910.